Chemistry Europe
European Chemical Societies Publishing

# Aminotroponiminates: Impact of the $NO_2$ Functional Group on Coordination, Isomerisation, and Backbone Substitution

Anna Hanft,[a] Dennis Rottschäfer,[a] Nele Wieprecht,[a] Felix Geist,[a] Krzysztof Radacki,[a] and Crispin Lichtenberg*[a]

**Abstract:** Aminotroponiminate (ATI) ligands are a versatile class of redox-active and potentially cooperative ligands with a rich coordination chemistry that have consequently found a wide range of applications in synthesis and catalysis. While backbone substitution of these ligands has been investigated in some detail, the impact of electron-withdrawing groups on the coordination chemistry and reactivity of ATIs has been little investigated. We report here Li, Na, and K salts of an ATI ligand with a nitro-substituent in the backbone. It is demonstrated that the $NO_2$ group actively contributes to the coordination chemistry of these complexes, effectively competing with the N,N-binding pocket as a coordination site. This results in an unprecedented *E/Z* isomerisation of an ATI imino group and culminates in the isolation of the first "naked" (i.e., without directional bonding to a metal atom) ATI anion. Reactions of sodium ATIs with silver(I) and tritylium salts gave the first N,N-coordinated silver ATI complexes and unprecedented backbone substitution reactions. Analytical techniques applied in this work include multinuclear (VT-) NMR spectroscopy, single-crystal X-ray diffraction analysis, and DFT calculations.

## Introduction

Bidentate N,N ligands such as amidinates,[1] diazadienes,[2] phenylenediamides,[3] β-diketiminates,[4] and aminotroponiminates[5] (ATIs) are versatile tools in coordination chemistry, synthesis, catalysis, redox-applications,[6] and materials science. A key factor contributing to the broad success of these ligand systems is the fact that the ligand periphery can be fine-tuned according to the steric and electronic requirements of the relevant field of application, while the metal atom resides in the N,N-binding pocket. This has led to remarkable findings, for example in the stabilisation of metal atoms with unusual oxidation states (e.g., $Mg^{I}$, $Al^{I}$),[7] in electronic structure determination of transition metal complexes,[3,8] in small molecule activation (e.g., $N_2$ activation by Ca complexes),[9] and in catalysis (e.g., hydroamination, dehydrocoupling, nitrene transfer).[4a,9b,10]

For aminotroponiminates (ATIs) in particular, reactions aiming at the installation of different types of substituents at the nitrogen atoms[11] and the ligand backbone[11c,12] have been developed, and their impact on structure and reactivity has been demonstrated (Figure 1). Systematic variations of nitrogen-bound substituents can be exploited to control the ability of ATI ligands to interact with metal atoms through the π-electrons of their ligand backbone (Figure 1a)[11h,13] and their catalytic activity in the polymerisation of ε-caprolactone.[13c]

With respect to backbone substitution, cooperative behaviour, for instance in reactions of group 13 ATI complexes with trityl species,[14] and reductively-induced reversible dimerisation reactions of alkali metal complexes have been reported (Figure1b,c).[15] Unforeseen backbone substitution reactions have also been reported in the context of NO disproportionation (Figure 1d).[16] In hydroamination catalysis, variations of the backbone substituents were shown to have a dramatic influence on the catalytic activity of zinc complexes. For nitro-substituted ATIs, it was suggested that $Zn\cdots O_2N$ interactions critically influence the catalytic activity,[12a,b] but such interactions have not yet been theoretically investigated or experimentally detected.

While the installation of electron-withdrawing substituents in the backbone of ATI ligands has been exemplified, and their impact on catalytic activities has been noted,[11c,12] the consequences of an electron-withdrawing substituent on the electronic and structural properties, coordination chemistry, and reactivity of ATI ligands has not yet been investigated in detail (Figure 1e). Somewhat surprisingly, this holds true for the entire range of backbone substituents in the large family of ATI complexes.[11c,12]

Herein, we report the synthesis, isolation and characterisation of nitro-substituted ATI complexes of the alkali metals Li, Na, and K, their isomerisation, their reactivity under oxidising conditions, and access to the "naked" ATI anion.

[a] *Dr. A. Hanft, Dr. D. Rottschäfer, N. Wieprecht, F. Geist, Dr. K. Radacki, Priv.-Doz. Dr. C. Lichtenberg*
*Institut für Anorganische Chemie*
*Fakultät für Chemie und Pharmazie*
*Julius-Maximilians-Universität Würzburg*
*Am Hubland, 97074 Würzburg (Germany)*
*E-mail: crispin.lichtenberg@uni-wuerzburg.de*

*Supporting information for this article is available on the WWW under https://doi.org/10.1002/chem.202102324*

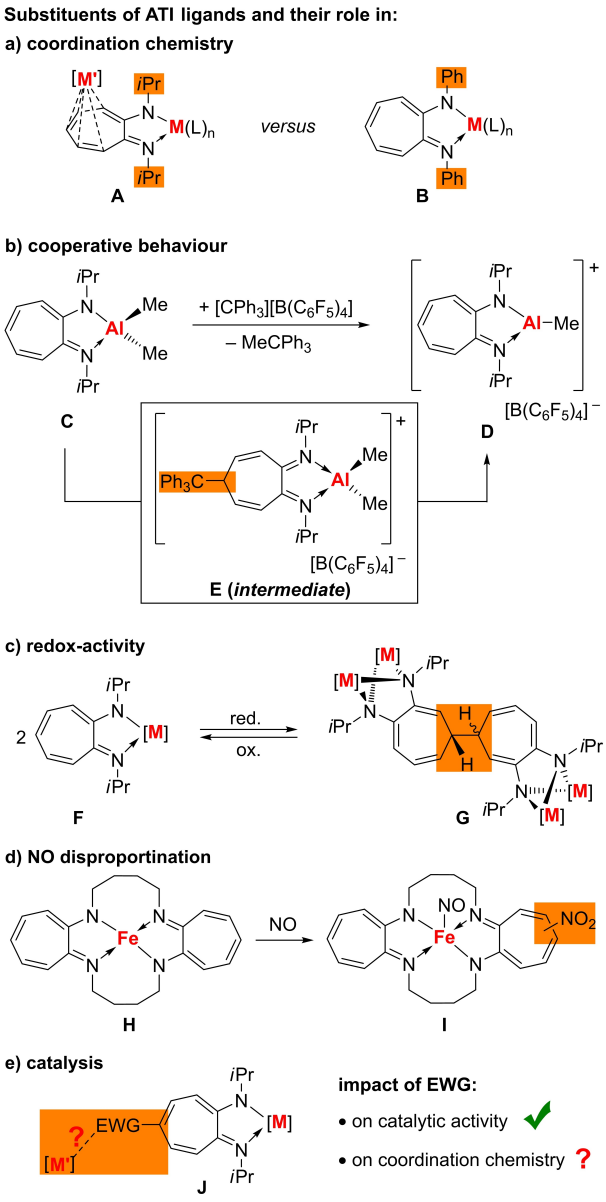


**Figure 1.** Substituents at the nitrogen atoms and at the backbone of ATI ligands and their role in various fields of research. EWG = electron-withdrawing group.

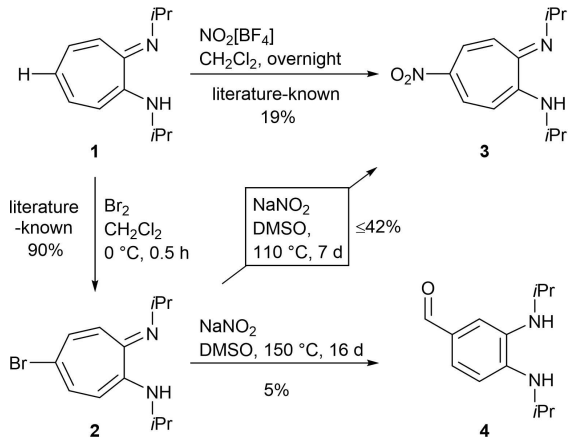


**Scheme 1.** Synthesis of **3** and **4**.

## Results and Discussion

### Ligand synthesis

H-$NO_2$-ATI$^{iPr/iPr}$ (**3**) was synthesised following a literature protocol by the reaction of **1** with $NO_2[BF_4]$ as a nitrating agent (Scheme 1).[12a] Since variations of the reaction conditions did not lead to an improvement of the low yield of 19% (see the Supporting Information), a two-step synthesis was targeted: **1** was brominated according to the literature,[12e] and the resulting 5-bromoaminotroponimine **2** was reacted with $NaNO_2$ in dimethylsulfoxide (DMSO, Scheme 1). Under optimised reaction conditions, **3** was obtained in isolated yields of up to 42% (38% over two steps), which varied, however, when the solvent was not freshly distilled prior to use, for instance (see the Supporting Information). Increasing the reaction time and temperature (150 °C, 16 d) drastically lowered the yield of **3** to < 5% and unexpectedly gave the aldehyde **4**, which was isolated in small yields of 5% and fully characterised. Compound **4** is the product of a ring contraction reaction. Related types of such transformations have been reported for halotropone, -tropolone and aminotropone derivatives in reactions with various nucleophiles in competition with substitution reactions.[17] However, a rearrangement of this type is without precedent for aminotropone imines.

Aminotroponimine **3** crystallises from *n*-pentane in the orthorhombic space group *Pbca* ($Z = 8$, Figure 2). The N1/2–C1/2 bonds (1.30 and 1.32 Å, respectively) are only slightly shorter than the analogous bonds of backbone-unsubstituted **1** (N1–C1, 1.31 Å; N2–C2, 1. 34 Å)[11e,18] and lie in between the typical N–C bond lengths of characteristic imine and amine units (1.28 and 1.35 Å, respectively).[19] This could be due to an increased delocalisation of the π-electrons caused by the influence of the electron-withdrawing $NO_2$ group. With bond lengths of 1.36 to 1.45 Å, the C–C bonds in the $C_7$ backbone

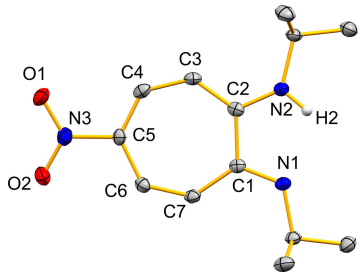


**Figure 2.** Solid-state molecular structure of **3**. Hydrogen atoms except for H2 are omitted for clarity. Displacement ellipsoids are depicted at the 50% probability level. Selected bond lengths [Å] and angles [°]: O1–N3 1.243(2), O2–N3 1.240(2), N1–C1 1.296(2), N2–C2 1.323(2), N3–C5 1.450(2), C1–C2 1.507(2), C2–C3 1.400(2), C3–C4 1.385(2), C4–C5 1.371(2), C5–C6 1.415(2), C6–C7 1.357(2), C7–C1 1.448(2), C1–C2–C3 126.9(2), C2–C3–C4 130.9(2), C3–C4–C5 130.2(2), C4–C5–C6 127.7(2), C5–C6–C7 128.6(2), C6–C7–C1 133.1(2), C7–C1–C2 122.6(2), N1–C1–C2–N2 1.15(2).

**Table 1.** Selected bond lengths [Å], angles between mean planes [°], and torsion angles [°] of compounds **5**-M, **6**-Na, and **7**.

| Bond/angle | **3** | **5-Li** | **5-Na** | **5-K** | **6-Na** | **6-K** | **7** |
|---|---|---|---|---|---|---|---|
| C–N*i*Pr | 1.296(2), 1.323(2) | 1.2889(18), 1.2908(18) | 1.293(2), 1.286(2) | 1.283(2), 1.291(2) | 1.2860(18), 1.2874(18) | 1.2820(18), 1.2782(18) | 1.279(3), 1.284(3) |
| C–$NO_2$ | 1.450(2) | 1.3669(19) | 1.378(2) | 1.375(2) | 1.3779(18) | 1.3710(16) | 1.395(3) |
| $\Delta_{max}$(C–C)[a] | 0.09 | 0.11 | 0.11 | 0.13 | 0.12 | 0.13 | 0.12 |
| ∡([C1–7]-[C1–2,N1–2]) | 1.0 | 26.1 | 27.0, 31.2 | 37.5 | 40.2 | 43.6 | 41.7 |
| ∡(N1–C1–C2–N2) | 1.1 | 29.7 | 32.8 | 47.0 | 54.3 | 61.6 | 54.6 |
| ∡ (C4–C5–N–$O^{cis}$) | 9.4 | 1.8 | 2.2 | 5.0 | 7.7 | 4.5 | 0.6 |

[a] the C1–C2 bond is excluded here, because single bond character can be expected to dominate.

(except for C1–C2) also lie in between characteristic C–C single and double bonds. However, with bond length differences between two adjacent bonds of $\Delta_{max}$(C–C) = 0.09 Å, a larger bond length alternation than in **1** ($\Delta_{max}$(C–C) = 0.07 Å)[18] is observed, indicating a lower delocalisation of the π-electron density due to the −I and −M effects of the nitro group (for a comparison with alkali metal complexes of **3**, also see Table 1). The N3–C5 bond (1.45 Å) is in the range of a typical N–C single bond. The N3–O bond lengths are identical within limits of error (1.24 Å) and elongated compared to bond lengths of characteristic nitro substituents (1.22 Å).[19] Similar to the parent compound **1**, the $C_7$ ring and the $C_2N_2$ plane of the amino imine unit in **3** are almost co-planar ([C1-2,N1-2]-[C1-7] = 1.05°). The C4–C5–N3-O1 torsion angle of 9.4(2)° as well as the O1–N3–O2 bond angle (121.5°), are similar to analogous angles in *para*-substituted nitrobenzene derivatives.[20]

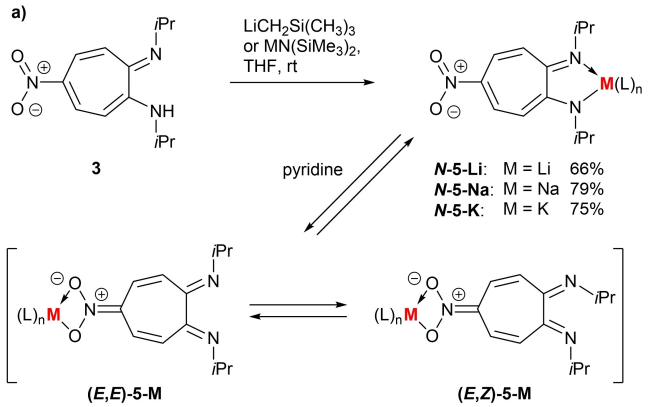


b)

$\Delta H^{rel}$ / $\Delta G^{rel}$ [kcal·mol$^{-1}$]

| M | ***N*-5-M-(py)$_2$** | **(*E*,*E*)-5-M-(py)$_2$** | **(*E*,*Z*)-5-M-(py)$_2$** |
|---|---|---|---|
| Li | 0.0 / 0.0 | +10.8 / +8.2 | +8.6 / +6.6 |
| Na | 0.0 / 0.0 | +7.7 / +4.4 | +5.5 / +1.4 |
| K | 0.0 / 0.0 | +5.4 / +3.4 | +2.2 / +1.3 |

**Scheme 2.** a) Synthesis of alkali-metal complexes **5-M** (with isomers ***N*-5-M**, **(*E*,*E*)-5-M**, and **(*E*,*Z*)-5-M**) and b) relative energies of different isomers according to DFT calculations. L = neutral ligand.

### Alkali-metal complexes

Starting from **3**, the alkali metal complexes [M($NO_2$-ATI$^{iPr/iPr}$)] (**5-M**, M = Li, Na, K) were synthesised (Scheme 2; the term "**5-M**" includes all isomers of these compounds, while the terms "***N*-5-M**", "**(*E*,*E*)-5-M**", and "**(*E*,*Z*)-5-M**" address specific isomers; see below). The complexes of the higher homologues Na and K proved to be poorly soluble in THF and precipitate during the synthesis in this solvent. The $^1$H and $^{13}$C NMR spectra of complexes **5-M** in [$D_5$]pyridine show a set of signals consistent with a $C_{2v}$-symmetric molecule in solution. In the case of **5-Na** and **5-K**, a second set of signals is detected after a few hours in solution, indicating the presence of a species with $C_1$ symmetry. We show that the $C_1$-symmetric species is the product of a metal migration from the N,N-binding pocket to the nitro group in the ligand backbone, followed by an unprecedented *E/Z* isomerisation of one ATI-imino group (i.e., formation of **(*E*,*Z*)-5-M**, see below; Scheme 2a). The isomerisation reactions reach their equilibria at ratios ($C_{2v}$/$C_1$) of 1.0:1.5 (Na) and 1.0:1.6 (K) after 3 d at room temperature in pyridine solution. Heating a pyridine solution of **5-Na** to 60 or 80 °C for four to seven days did not lead to a significant change of the isomer ratio, and after several days at 80 °C only the decomposition of the compound to protonated ligand **3** was observed. When the synthesis of **5-K** was performed in [$D_5$]pyridine, NMR spectroscopic monitoring revealed the instant formation of both isomers, that is, the exclusive formation of ***N*-5-K** in reactions using THF as a solvent is most likely the result of rapid precipitation of the product prior to isomerisation. The solution $^{15}$N-$^1$H HMBC NMR spectrum of **5-K** exhibits cross-signals at $\delta$ = −53.9 ppm for the nitrogen atoms of the $C_{2v}$ symmetric compound, and signals at $\delta$ = −41.2 ppm and −32.6 ppm for the $C_1$ symmetric compound. All these signals lie in a typical range for imino groups,[21] suggesting a shift of the π-electron density towards the nitro group (Scheme 2a). In the solution $^1$H,$^1$H NOESY NMR spectra of **5-Na** and **5-K**, one C*H*Me$_2$ group of the $C_1$ symmetric isomer, **(*E*,*Z*)-5-M**, shows no cross signal to the protons of the ATI backbone (in contrast to the other C*H*Me$_2$ units in **5-Na** and **5-K**), indicating the *Z* configuration of the respective imino group.

In order to exclude the possible influence of the formation of a monomer/oligomer mixture on NMR spectroscopic signal patterns, a $^1$H,$^1$H DOSY NMR spectrum of **5-K** was recorded. The diffusion coefficients were determined to be $4.14\times10^{-10}$ and $4.34\times10^{-10}$ m$^2$·s$^{-1}$ for the $C_{2v}$- and the $C_1$-symmetric species,

respectively, showing that in solution these compounds possess very similar to identical molar masses. This supports the assumption of *E,E*-to-*E,Z* isomerisation. The experimental results on the equilibrium isomerisation of **5-M** in the case of M = Na, K, but not for M = Li are further supported by DFT calculations (B3LYP, 6–311G(d,p) [Na, K], 6–31G(d,p) [all other atoms]) with a pyridine solvent model and dispersion corrections; Scheme 2b). The calculations indicate that for the pyridine-solvated model compounds [M($NO_2$-ATI$^{iPr/iPr}$)(py)$_2$] (M = Li, Na, K), ***(E,Z)*-5-M-(py)$_2$** is slightly higher in energy than ***N*-5-M-(py)$_2$** for M = Li ($\Delta G$ = 6.6 kcal·mol$^{-1}$), while these isomers are almost isoenergetic for M = Na ($\Delta G$ = 1.4 kcal·mol$^{-1}$) and M = K ($\Delta G$ = 1.3 kcal·mol$^{-1}$).

As both the sodium and the potassium complex are poorly soluble in polar solvents such as THF and only moderately soluble in pyridine, attempts were made to improve the solubility properties by complexation with crown ethers. For this purpose, **5-Na** and **5-K** were treated with 1 equivalent of 15-crown-5 and 18-crown-6, respectively, in THF (Scheme 3a). This led to a complete dissolution of the solid material within one hour. Thus, the formation of the corresponding crown ether complexes [Na(15-crown-5)($NO_2$-ATI$^{iPr/iPr}$)] (**6-Na**) and [K-(18-crown-6)($NO_2$-ATI$^{iPr/iPr}$)] (**6-K**) can be assumed. Moreover, **5-Na** was treated with 2 equiv. 12-crown-4 to give THF-soluble [Na(12-crown-4)$_2$][$NO_2$-ATI$^{iPr/iPr}$] (**7**). All crown ether complexes, like their parent compounds, show two sets of signals in their $^1$H and $^{13}$C NMR spectra, which can be assigned to two *E,E* isomers (***N*-6-M** and/or **(*E,E*)-6-M**) and one *E,Z* isomer (**(*E,Z*)-6-M**), respectively (**6-Na**: 1.0:1.9, **6-K**: 1.0:1.5). The $^{15}$N NMR signals of **6-Na**, which were determined using $^1$H,$^{15}$N HMBC NMR spectroscopy, again reveal two sets of resonances, one of which indicates the presence of two inequivalent imino groups (*E,E* isomer: $\delta$ = −63.2 ppm, *E,Z* isomer: $\delta$ = −51.0 ppm, −42.3 ppm). Furthermore, the signals of the nitro group could be detected at $\delta$ = −25.6 (*E,E* isomer) and −31.6 ppm (*E,Z* isomer), respectively. For steric reasons and due to the appearance of the *E,Z* isomers, the coordination of the [M(crown ether)]$^+$ units in **6-M** is expected to occur preferentially via the nitro group of the ATI ligand. However, $^1$H,$^1$H NOESY NMR spectra of these compounds also reveal cross signals between the *i*Pr groups of the ATI ligand and the ethylene units of the crown ethers. Based on DFT calculations (see below) and in congruency with the coordination chemistry of other ATI complexes of Na and K,[13] we suggest the accessibility of isomers in solution, in which the alkali metal cation interacts with π-electron density of the ATI backbone.

DFT calculations on the sodium crown ether complexes **(*E,Z*)-6-Na** and **(*E,Z*)-7** indicate that their formation from pyridine-solvate ***N*-5-Na-(py)$_2$** is energetically favourable by $\Delta G$ = −18.7 kcal·mol$^{-1}$ (formation of **6-Na**) and $\Delta G$ = −24.5 kcal·mol$^{-1}$ (formation of **7**), respectively. Among the relevant isomers of **6-Na**, **(*E,Z*)-6-Na** is energetically most favourable, which is consistent with the solid-state structure (Figure 2). In congruency with results from solution NMR spectroscopy, three other isomers are only slightly higher in energy. These are two isomers with the imino groups in *E,E* configuration (**(*E,E*)-6-Na**: $\Delta G$ = +1.1 kcal·mol$^{-1}$ and ***N*-6-Na**: $\Delta$G = +2.4 kcal·mol$^{-1}$) and one isomer with the imino groups in the *E,Z* configuration in which the sodium cation interacts with the π-electrons of the ligand backbone (***π*-6-Na**: $\Delta G$ = + 3.7 kcal·mol$^{-1}$; for a more detailed presentation see the Supporting Information).

For compound **7** with its "naked" ATI anion, the *E,Z* configuration found in the solid state is lower in energy than the (*E,E*)-configuration by $\Delta$G = −3.7 kcal·mol$^{-1}$. This is also corroborated by $^1$H NMR spectroscopy, which reveals an **(*E,E*)-7**:**(*E/Z*)-7** isomeric ratio of 1.0:1.3.

From a mechanistic point of view, the *E/Z* isomerisation of the C=N double bond can proceed via an inversion, a rotation, or a variety of pathways that lie between these two extremes.[22] Calculations have shown that such isomerisations tend to proceed via an inversion mechanism if the double bond carries substituents with positive Hammett parameters ($\sigma_m$).[22b] For compound **7**, an almost linear transition state ($\alpha$ = 169.5°) was calculated for a configuration change from *E,E* to *E,Z* with an energy barrier of $\Delta G^{\neq}$ = +22.9 kcal·mol$^{-1}$ (Scheme 3b). This suggests that the electron-withdrawing properties of the nitro

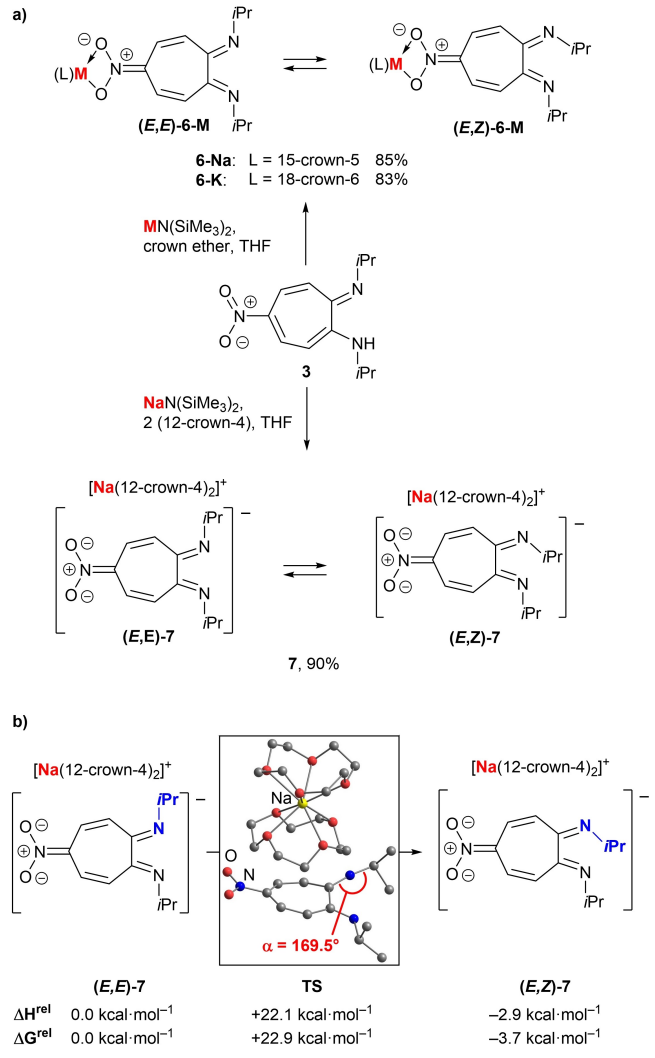


**Scheme 3.** a) Synthesis of sodium and potassium crown ether ATI complexes **6**-M and **7**. b) DFT-calculated thermodynamic and kinetic parameters for the *E/Z* isomerisation of compound **7**.

substituent significantly influence the isomerisation mechanism, as the *N*-isopropyl substituent is attributed a slightly negative Hammett parameter due to its electron-pushing properties.

The solid-state structures of the alkali metal complexes [**5-Li**(py)]$_\infty$ (Figure 3 and Figure S41 in the Supporting Information), [**5-Na**(py)]$_\infty$ (Figures 3 and S42), and [**5-K**(py)]$_\infty$ (Figures 3 and S43) were elucidated by sc-XRD analysis. All compounds were crystallised from pyridine/*n*-pentane solvent systems and show some structural similarities with respect to the ATI ligand (cf. Table 1): the C–N*i*Pr bond lengths within each compound are identical within limits of error (1.28–1.29 Å) and in the range of N=C double bonds of imino groups attached to arenes.[19] The C–C bond lengths in the ATI backbone range between values expected for typical C–C single and double bonds. However, the bond length alternation of two adjacent C–C bonds ($\Delta_{max}$(C–C) = 0.11–0.13 Å) is larger than that in **3** ($\Delta_{max}$-(C–C) = 0.09 Å). Moreover, C–$NO_2$ bond lengths (1.37-1.38 Å) and the C4–C5–N–$O^{cis}$ torsion angles (1.8–5.0°) are considerably smaller than those in **3** (1.45 Å and 9.4°). Whereas the neutral ligand **3** shows an essentially planar $C_7N_2$ group, the ATI core in the alkali metal complexes **5-M** is twisted. This is reflected by large N–C–C–N torsion angles (29.7–47.0°) and large interplanar angles ([C1–7]-[C1–2,N1–2], 26.1–37.5°), the latter being the highest values observed for (half-)metal ATI complexes.[5b,23] All these findings support a shift of the π-electron density towards the electron-withdrawing nitro group, which was already suspected on the basis of the NMR spectroscopic data (see above). The introduction of an (electron-withdrawing) substituent at the ATI backbone can thus be used as a tool to push the limits of ATI backbone flexibility.

The metal cations in **5-M** are five-coordinate due to interactions with the N,N-binding pocket, $NO_2$ groups of neighbouring ATI units, and one pyridine ligand. This leads to a distorted trigonal bipyramidal coordination geometry for **5-Li** ($\tau = 0.63$, with N1 and O1′ occupying the axial positions) and to distorted square pyramidal coordination geometries for **5-Na** and **5-K** ($\tau = 0.46$ with O1′ in the apical position and $\tau = 0.30$ with N1 in the apical position). In **5-Li** and **5-Na**, the interactions of the metal cations with the $NO_2$ groups of neighbouring formula units lead to the formation of one-dimensional coordination polymers in the solid state, which extend along a $2_1$-screw axis in the direction of the crystallographic *b*-axis (Figures S41b and S42b). This results in a $\mu_2$-(M-$\kappa_2$-N)-(M′-$\kappa_2$-O) coordination mode for both compounds. In compound **5-K**, each metal cation interacts with two oxygen atoms of two different nitro groups. The bridging coordination mode of the ATI ligand between three different metal centres via the N,N-binding pocket and a backbone substituent is unprecedented in the coordination chemistry of ATI complexes[5] and results in the formation of a complex coordination polymer in the solid state (for a more detailed presentation see the Supporting Information).

The solid-state structures of the crown ether compounds **6-Na**, **6-K**, and **7** have also been elucidated by sc-XRD analysis of samples obtained from pyridine/*n*-pentane (**6-Na**, **7**) or THF/*n*-pentane (**6-K**) solvent systems (**6-Na**: monoclinic, $P2_1/c$, $Z = 4$,

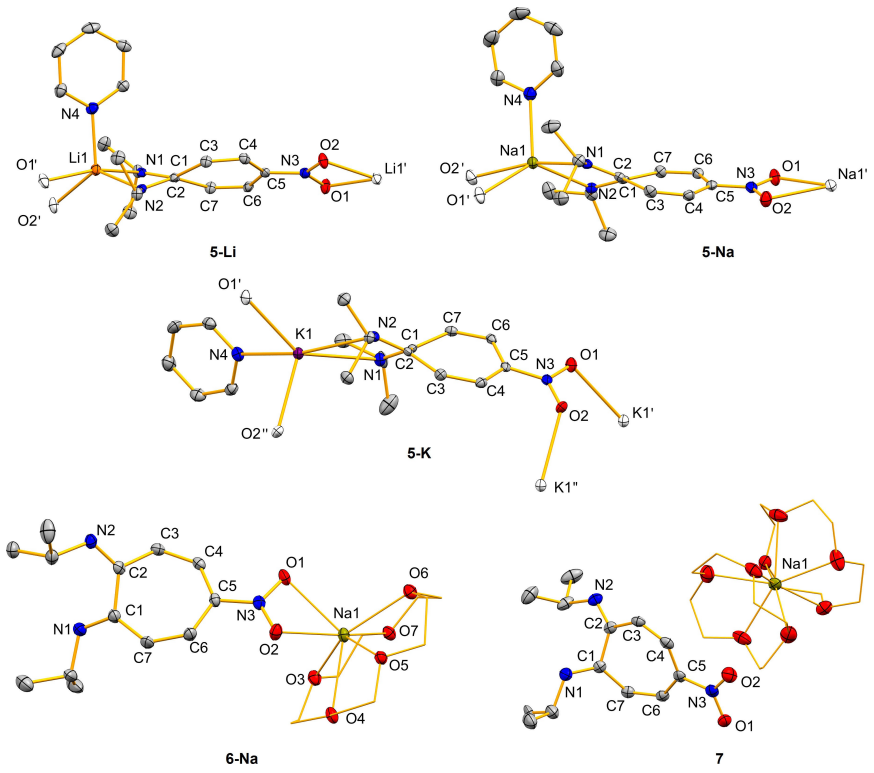


**Figure 3.** Solid-state structures of alkali-metal complexes **5**-M, **6**-Na, and **7**. Hydrogen atoms are omitted and the carbon atoms of crown ethers are shown as wireframe for clarity. Displacement ellipsoids are depicted at the 50% probability level.

Figures 3 and S44; **6-K**: monoclinic, *C*2/*c*, *Z* = 8, Figure S45). **6-Na** and **6-K** show monomeric structures in the solid state. The metal cations interact with the crown ether molecules and the two oxygen atoms of the nitro group of the ligand, resulting in irregular coordination geometries with coordination numbers of seven (Na) and eight (K). Remarkably, this leads to an unoccupied N,N-binding pocket of the ligand, which is unprecedented in chemistry of anionic ATI complexes and further extends the rich coordination chemistry of this ligand family. The absence of a metal atom in the N,N-binding pocket allows for the *E*/*Z* isomerisation of an imino group, which is in agreement with results from solution NMR spectroscopic analyses and DFT calculations and for the first time structurally authenticated in compounds **6-M**. Analogous to the crown ether-free parent compound, the bonding parameters of the ligand framework for both compounds indicate a shift of π-electron density towards the nitro group and an increased localisation of the π-electrons compared to ATI complexes without backbone substitution (Table 1).

While anionic hydrocarbon ligands such as cyclopentadienide[24] or indenide[25] without directional bonding interactions to a metal atom have been reported to the literature, such species have – to the best of our knowledge – eluded isolation and full characterisation for anionic ligands with an *N,N*-binding pocket, such as amidinates, β-diketiminates, and ATIs. This may be due to the fact that the incorporation of electronegative nitrogen atoms into anionic hydrocarbon moieties induces a significant dipole moment, which makes anion-metal interactions favourable. Even in the presence of chelating neutral ligands M–N interactions commonly persist, for instance through the formation of unusual ate complexes.[13c] Thus, it is remarkable that complexation of the Na atom in **5-Na** with two equiv. of 12-crown-4 leads to the formation of a free ligand anion that does not undergo any directional bonding interactions to the $[Na(12\text{-crown-}4)_2]^+$ complex cation (**7**: monoclinic, $P2_1/c$, $Z = 4$, Figures 3 and S46). Despite the lack of coordination of the metal atom to the ligands, complex salt **7** shows a twist ($[C_7]$-$[C_2N_2]$) of 41.7° for the ATI framework. As in compounds **6-M**, the N–C and C–C bond lengths also indicate a shift of π-electron density towards the nitro group in **7** (Table 1).

## Silver(I) complexes

The redox-activity and tuneability of ATIs as ligands in alkali metal, rhodium, and cationic bismuth complexes has been documented in recent years.[5b,11h,15,26] Cyclic voltammetry studies on compounds **3** and **5**-M, however, did not indicate fully reversible redox events in THF / 0.1 M $[N(nBu)_4][PF_6]$ at ambient temperature and scan rates of 250 $mV \cdot s^{-1}$ (for details see the Supporting Information). Nevertheless, the accessibility of a "naked" ATI anion in nitro-substituted compounds prompted us to investigate the one-electron oxidation of ATIs bearing nitro groups in the ligand backbone. While reactions of **5-Na**, **6-Na**, and **7** with $[Fe(Cp)_2]Cl$ or $NOSbF_6$ (and in some attempts also in the presence of TEMPO (2,2,6,6-tetramethylpiperidinyloxyl) or diphenyl ditelluride as radical trapping reagents) gave the neutral ligand **3** and sodium salts as the only identifiable products (Table S4), reaction of **5-Na**, **6-Na**, and **7** with one and two equivalents, respectively, of $AgBF_4$ led to new ATI complexes according to NMR spectroscopic reaction monitoring (Scheme 4). No indications for the formation of radical species or the products of radical coupling (as reported for ATI species under reducing conditions)[15] could be obtained. The NMR spectroscopic analysis showed signal sets typical of $C_{2v}$-symmetric ATI units in all cases and (together with the stoichiometric ratios that were necessary to generate these species and the soft character of $Ag^+$[27]) justify the structural assignments shown in Scheme 4. While a satisfying separation of the $NaBF_4$ by-product from compound **8** could not be achieved, only traces (< 1 %) of this by-product could be detected in isolated and re-crystallised samples of **9** and **10**.

The structural assignments for **8**–**10** were confirmed by sc-XRD analyses (Figure 4) and selected parameters are summarised in Table 2. Compound **8** crystallises in the triclinic space group $P\bar{1}$ with $Z = 2$. The structure shows the $\kappa_2$-*N* coordination mode most commonly observed for ATI complexes. The silver atom is found in a distorted trigonal-planar coordination geometry due to interactions with the $N^{ATI}$ atoms and a pyridine molecule. The distortion is due to the bite angle of the ATI binding pocket (N1–Ag1–N2, 72°). The Ag–N bond lengths (2.17–2.27 Å) are in a similar range as those in structurally related pyridylpyrrolide,[28] 2,2′-bipyridine silver complexes[29] and silver-β-diketaminates,[30] which also show three-coordinate silver atoms. Compared to the alkali metal complexes **5-M**, **6-M**, and **7**, the bonding parameters of the ligand indicate a less pronounced shift of π-electron density towards the nitro group in **8**. The N3–C5 bond (1.43 Å) has primarily single-bond character (alkali metal-ATI complexes: N3–C5, 1.37–1.40 Å) and the maximum bond length difference of two adjacent C–C bonds in **8** ($\Delta_{max}$(C–C) = 0.10 Å) is slightly lower than in the alkali metal derivatives ($\Delta_{max}$(C–C) = 0.11–0.13 Å). The increased delocalisation of the π-electrons is also reflected by a smaller angle between the idealised planes [C1-2,N1-2,Ag] and [C1–C7] (17.1°).

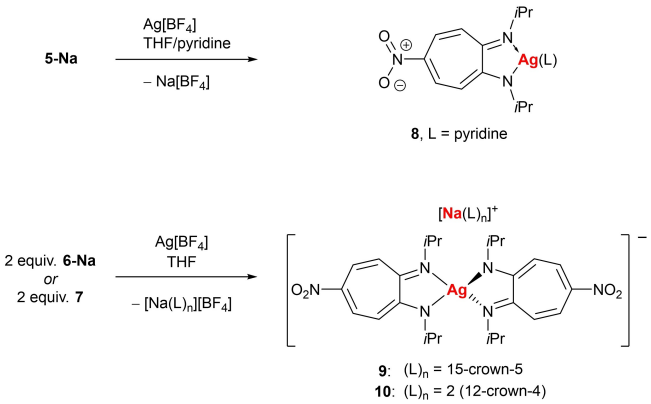


**Scheme 4.** Synthesis of silver(I) complex **8** and sodium argentate(I) complexes **9** and **10**.

 

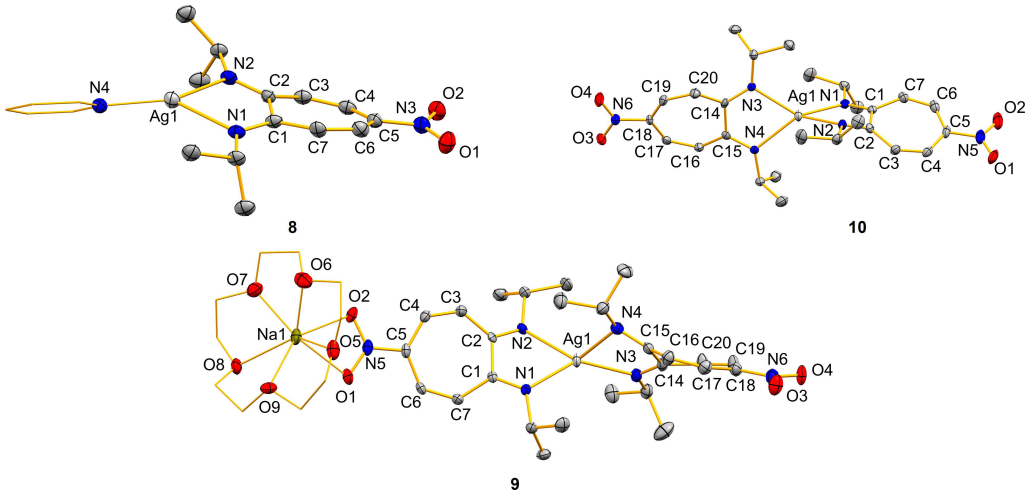


**Figure 4.** Solid-state molecular structures of **8**, the anionic part in **9**, and **10**. Hydrogen atoms are omitted and pyridine as well as crown-ether carbon atoms are depicted as wire model for clarity. Thermal displacement ellipsoids are depicted at the 50% probability level.

**Table 2.** Selected bond lengths [Å], bond angles [°], dihedral angles [°], and angles between mean planes [°] of silver complexes **8**, **9** and **10**.

| Bond/angle | **8** | **9** | **10** |
|---|---|---|---|
| C–N*i*Pr | 1.2940(1), 1.3035(1) | 1.295(3), 1.297(4), 1.303(4), 1.303(4) | 1.299(4), 1.296(4), 1.292(4), 1.303(4) |
| C–$NO_2$ | 1.4254(1) | 1.387(4), 1.400(4) | 1.407(4), 1.403(4) |
| Ag–N*i*Pr | 2.273(3), 2.249(3) | 2.284(3), 2.297(2), 2.211(3), 2.437(3) | 2.261(3), 2.344(2), 2.304(2), 2.299(3) |
| $\Delta_{max}$(C–C) | 0.09 | 0.10 | 0.09 |
| ∡([C1-7]-[C1-2,N1-2,Ag1]) | 17.0 | 26.3 | 24.0 |
| ∡([C14-20] – [C14-15,N3-4,Ag1]) | – | 31.5 | 26.2 |
| ∡(N1–C1–C2–N2) | 19.3 | 30.9 | 26.8 |
| ∡(N3–C14–C15–N4) | – | 35.4 | 30.6 |
| ∡(C4–C5–N–$O^{cis}$)[a] | 10.6 | 0.2 | 5.4 |
| ∡(C17–C18–N6–O3) | – | 7.0 | 7.0 |

[a] For compound **8**, ∡(C4–C5–N3–O1/2) is discussed and for compounds **9** and **10**, ∡(C4–C5–N5–O1/2) is discussed.

Compounds **9** and **10** crystallise in the monoclinic space group $P2_1/n$ with $Z=4$ and in the triclinic space group $P\bar{1}$ with $Z=2$, respectively. In both cases, the silver atoms are situated in the N,N-binding pockets of two ATI ligands. This results in a distorted tetrahedral coordination geometry around Ag, the distortion being due to the small bite angle of the ATI ligand (**9**: N1/3–Ag1–N2/4 71.80(9)–72.69(10)°; **10**: N1/3–Ag1–N2/4 71.31(9)–71.58(8)°). Unlike **10**, in which there is no directional bonding interaction between the complex cation and anion, the $[Na(15\text{-crown-}5)]^+$ moiety in **9** coordinates to the nitro group of one ATI ligand. The Ag–N bond lengths (2.21 to 2.44 Å) are in a similar range as those of related silver complexes with nitrogen donor ligands and a coordination number of four for the silver atoms.[31] Compared to the monometallic, mononuclear complex **8** (Ag–$N^{ATI}$, 2.25–2.27 Å), the Ag–N bonds are elongated on average, which can be attributed to the higher coordination number of the silver atom as well as the negative charge of the $[Ag(NO_2\text{-}ATI^{iPr/iPr})_2]^-$ unit in the heterobimetallic complexes **9** and **10**. In both, **9** and **10**, the Ag–N bond lengths differ significantly in one ATI ligand (2.26–2.34 Å), whereas they are identical within limits of error in the other ATI unit (2.28–2.30 Å); that is, this effect is not due to the Na-$O_2$N interactions, which are present in **9**, but absent in **10**. The remaining bonding parameters in all ATI units of **9** and **10** are similar to each other, suggesting similar electronic situations despite the differences in Ag–N bond lengths.

Examples of silver-containing ATI complexes in the literature are rare and limited to germanium and tin complexes $[M(ATI^{R/R})X][Ag(HB(3,5\text{-}(CF_3Pz)_3]$ (M = Ge, Sn; X = Cl, I, $N_3$, $O_3SCF_3$; R = Me, *n*Pr; Pz = pyrazolyl),[23a,32] and thio- and selenogermanone-coordinated silver complexes $[(Ph\text{-}EGe(ATI^{tBu/tBu})(AgI)]_2$ (E = S, Se).[33] In all these examples, the ATI ligand does not coordinate to the silver atom, but Ge/Sn–Ag bonds are formed, or adduct formation with GeE→AgI units occurs. Compounds **8**–**10** are thus the first representatives of Ag-ATI complexes in which the silver atom is coordinated as a central atom by the N,N-binding pocket. The synthesis of ATI ate species **9** and **10** parallels that of previously reported homo- and heterobimetallic alkali metal ATI ate complexes.[13c]

## Electrophilic aromatic substitution

NMR-spectroscopic monitoring of the reaction between **7** and $Ph_3C[BF_4]$ in $[D_5]$pyridine showed signals of **3** and of an unknown ATI species (Table S4, entry 10). Based on the signal

pattern observed in $^{1}H$ and $^{13}C$ NMR spectra, the compound features an unsymmetrically substituted backbone. An analogous reaction of **7** with $Ph_3CCl$ in THF gave the same species, which was unambiguously identified as [Na(12-crown-4)$_2$][(3-$Ph_3C$-5-$NO_2$-ATI$^{iPr/iPr}$)] (**11**) by sc-XRD analysis (Scheme 5, Figure 5). The ionic complex **11** crystallises in the monoclinic space group $P2_1/n$ ($Z=4$, Figure 5). In analogy to the structure of the reactant **7**, the trityl-substituted ATI ligand is present as a free anion that does not undergo directional bonding interactions with the complex cation and shows an *E,Z* configuration of the imino groups. The coordination polyhedron around the sodium atom is a distorted antiprism with the oxygen atoms of two crown ether molecules as coordination points. The N1/2–C1/2 bond lengths of 1.27-1.29 Å are in the same range as those of **7**, the N3–C5 (1.38 Å) bond is slightly shorter (**7**: 1.40 Å). The maximum bond length difference of two adjacent C–C bonds is also slightly larger (**11**: $\Delta_{max}$(C–C): 0.15 Å; **7**: $\Delta_{max}$(C–C): 0.12 Å) and the out-of-plane twist of 45.0° is stronger than that in the parent compound **7** ([C1–C7]-[C1-2,N1-2]: 41.7°). The shift of the π-electron density towards the nitro group is thus favoured by the +I effect of the triphenylmethyl substituent. Furthermore, it can be assumed that the strong twisting of the ATI framework

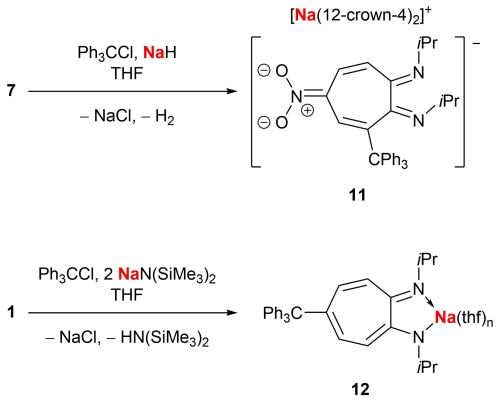


**Scheme 5.** Syntheses of 3-$CPh_3$-substituted ATI complexes **11** and **12**.

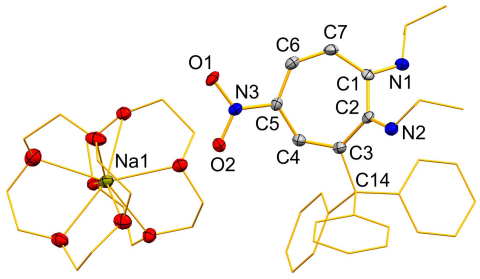


**Figure 5.** Solid-state molecular structure of **11**. Hydrogen atoms are omitted and carbon atoms of the crown ether moiety as well as the $CPh_3$ substituent are depicted as wire model for clarity. Displacement ellipsoids are depicted at the 50% probability level. O1–N3 1.2796(3), O2–N3 1.2787(4), N1–C1 1.2901(3), N2–C2 1.2734(3), N3–C5 1.3752(4), C1–C2 1.5203(7), C2–C3 1.4933(3), C3–C4 1.3407(4), C4–C5 1.4459(4), C5–C6 1.4219(5), C6–C7 1.3526(4), C7–C1 1.4540(3), C3–C14 1.5586(4), O1–N3-O2 118.552(41), O1–N3–C5 120.850(39), O2–N3–C5 120.597(38), N1–C1–C2 114.109(35), N2–C2–C1 124.887(36).88888

is additionally caused by the spatial proximity of the sterically demanding $Ph_3C$ substituent and the *iso*propyl group. Thus, the trityl salt does not act as an oxidant, but reacts with the ATI backbone in an electrophilic aromatic substitution reaction (Scheme 5).

The introduction of a triphenylmethyl group into the ATI backbone could first be demonstrated by Jordan et al. in the reaction of group 13 metal-ATI complexes [M(ATI$^{iPr/iPr}$)R$_2$] (M = Al–In, R = alkyl) with a trityl salt.[5b,14a,b,34] In this process, an electrophilic addition of the carbocation to the C5 position with the formation of a neutral diimine ligand skeleton occurs. An increase in temperature (to −40 °C for M = Al or to +80 °C for M = Ga, In), however, leads to rupture of the $C^{ATI}$–$CPh_3$ bond through the elimination of $RCPh_3$ (or $HCPh_3$ and an olefin if R contains β-H atoms), giving a cationic ATI complex with an unsubstituted ATI backbone as the final product (cf. Figure 1b).

In contrast to this cooperative behaviour of the ATI ligand observed in the literature, the reaction of **7** with a trityl salt yields a backbone $Ph_3C$-substituted complex. In the course of this reaction, 0.5 equivalents of the employed crown ether complex act as a base, which is necessary for the abstraction of the proton from the intermediately formed, but so far undetected σ-complex. This leads to the formation of the $CPh_3$-substituted crown ether complex **11** and the protonated ligand **3** (Table S4, entries 10 and 11). In principle, a radical reaction pathway would also be conceivable, in which first an electron is transferred from the ATI ligand to the trityl salt and then the σ-complex is generated by radical recombination. This scenario seems unlikely, however, because in an independent model reaction, Gomberg's dimer ($Ph_3C$–$C_6H_5$=$CPh_2$) did not react with the ATI ligand **3**.

Functionalisations in the C5 position in the ATI backbone of metal-free ligands are possible by an electrophilic aromatic substitution and have granted access to a broad variety of aminotroponimines.[12a,c,e] The transfer of a sterically demanding $Ph_3C$ group by reaction of the 5-$NO_2$-ATI complex **7** with $Ph_3CCl$ describes the first direct electrophilic aromatic substitution on an ATI complex.[16] Because the abstraction of a proton is required during the reaction, the sodium base NaH was employed in the rational synthesis of **11**. NMR spectroscopic monitoring of the reaction showed complete conversion to the desired product **11** (Scheme 4), which was isolated as an orange solid and fully characterised. In order to allow statements about whether an electrophilic aromatic substitution with trityl chloride is due to the already modified electronics of the ATI ligand caused by the nitro group in the C5 position, the backbone-unsubstituted sodium complex [Na(ATI$^{iPr/iPr}$)] was also investigated. For this purpose, the neutral ligand **1** was reacted with 1 equiv. of $Ph_3CCl$ and 2 equiv. of NaN(SiMe$_3$)$_2$ (Scheme 4). The complex [Na(5-$Ph_3C$-ATI$^{iPr/iPr}$)] (**12**) was isolated in good yields (73%). The NMR spectroscopic characterisation and elemental analysis are consistent with the formation of a complex substituted in the C5 position. The electrophilic aromatic substitution of sodium ATI complexes (isolated or prepared in situ) thus represents a simple route to functionalised complexes without complex purification steps.

Compound **12** crystallises from a THF/*n*-pentane mixture at −30 °C in the triclinic space group $P\bar{1}$ (Figure S51). While the quality of the crystallographic data is not sufficient for a discussion of bonding parameters, it serves as a proof of connectivity.

## Conclusion

In conclusion, a new synthetic pathway to the known backbone-$NO_2$-substituted aminotroponimine H-$NO_2$-ATI$^{iPr/iPr}$ (**3**) has been developed. Its alkali metal complexes (Li, Na, K) have been synthesised, isolated and fully characterised, revealing unforeseen aspects of aminotroponiminate (ATI) chemistry: i) the $NO_2$ substituent that was previously reported to modify the electronic structure of the ATI ligand (and to be innocent in terms of coordination chemistry) can act as a coordination site, thereby turning the ATI species into a ditopic ligand; ii) the $NO_2$ group can compete with the ATI–N,N-binding pocket as a coordination site to an extent that $NO_2$-M interactions can be preferred over N–M interactions; iii) extrusion of the metal centre from the N,N-binding pocket induces an unprecedented *E*/*Z* isomerisation of one imino group of the ATI ligand; iv) the ditopic nature of **3** can be exploited for the synthesis of heterobimetallic complexes; v) the electron-withdrawing nature of the $NO_2$ moiety allowed the first isolation and full characterisation of a "naked" ATI anion (i.e., an ATI anion without directional bonding interactions to a metal centre). Attempts to subject $NO_2$-substituted ATI complexes to selective one-electron oxidation reactions were unsuccessful to date. In addition to rapid H-atom transfer (to regenerate the neutral ligand), $Ag^+$ coordination (to give the first examples of silver ATI complexes) and electrophilic aromatic substitution in the ATI backbone (resulting in the introduction of $CPh_3$ substituents) were identified as favourable reaction pathways under (formally) oxidative conditions. It is anticipated that the ditopic nature of $NO_2$-substituted ATI ligands, the identification of the ATI-*N,N*-binding pocket as a potentially hemilabile coordination site, the accessibility of "naked" ATI anions, and the facile installation of additional carbon-based substituents in the ATI backbone will foster further developments in the complex design, coordination chemistry, and catalysis with the growingly versatile ATI ligand family and related species.

## Experimental Section

**General**: All air- and moisture-sensitive manipulations were carried out by using standard vacuum-line Schlenk or glove box techniques in an atmosphere of purified argon. Solvents were degassed and purified, according to standard laboratory procedures. NMR spectra were recorded on a Bruker instrument operating at 400 MHz with respect to $^1$H. All chemical shifts ($\delta$) are reported in ppm. $^1$H and $^{13}$C{$^1$H} NMR chemical shifts are reported relative to $SiMe_4$ by using the residual $^1$H and $^{13}$C chemical shifts of the solvent as a secondary standard. NMR chemical shifts of heteroatoms are reported as follows: $^7$Li relative to 1 M LiCl in $D_2O$,$^{15}$N relative to $CH_3NO_2$ (90% in $CDCl_3$), and $^{23}$Na relative to 1 M NaCl in $D_2O$. Unless stated otherwise, NMR spectra were recorded at 298 K. Elemental analyses were performed on a Leco or a Carlo Erba instrument. For MS analyses, an Exactive plus instrument (Thermo Scientific) was used. Cyclic voltammograms were recorded by using a Gamry Instruments Reference 600 potentiostat at room temperature (RT) in THF containing 0.1 M $[N(nBu)_4][PF_6]$, unless otherwise noted. A standard three-electrode cell configuration was employed by using a platinum disk working electrode, a platinum wire counter electrode, and a silver wire separated by a Vycor tip as the reference electrode. Formal redox potentials are referenced to the ferrocene/ferrocenium redox couple. Single crystals suitable for X-ray diffraction were coated with perfluorinated polyether oil in a glove box, transferred to a nylon loop, and then transferred to the goniometer of a diffractometer equipped with a molybdenum ($\lambda$ = 0.71073 Å) X-ray tube. The structures were solved using the intrinsic phasing method, completed by Fourier synthesis and refined by full-matrix least-squares procedures.

Deposition Numbers 2092742, 2092743, 2092744, 2092745, 2092746, 2092747, 2092748, 2092749, 2092750, 2092751, 2092752, 2092753 contain the supplementary crystallographic data for this paper. These data are provided free of charge by the joint Cambridge Crystallographic Data Centre and Fachinformationszentrum Karlsruhe Access Structures service.

**Computational details**: DFT calculations were performed with the Gaussian program by using the 6–31G(d,p)[35] (H, Li, C, N, O) and the 6–311G(d,p)[35–36] (Na, K) basis set and the B3LYP functional.[37] The D3 version of Grimme's dispersion model with the original D3 damping function and a pyridine polarisable continuum solvent model were applied.[38] Frequency analyses of the reported minimum structures and the transition state showed no imaginary frequencies and one imaginary frequency, respectively. Thermodynamic parameters were calculated at a temperature of 298.15 K and a pressure of 1.00 atm. Further details are given in the Supp. Inf. Cartesian coordinates of optimised structures are provided in .xyz format.

**H-$NO_2$–ATI$^{iPr/iPr}$ (3)**: $NaNO_2$ (256 mg, 3.71 mmol) was added to a solution of Br-ATI$^{iPr/iPr}$ (**2**, 1.00 g, 3.53 mmol) in DMSO (20 mL). The mixture was stirred at 110 °C for 7 d, and extracted with a mixture of $H_2O$ (150 mL) and MTBE (150 mL). The aqueous phase was extracted with MTBE (3×100 mL) and the combined organic phases were washed with saturated NaCl solution (40 mL), and dried over $MgSO_4$. The solvent was evaporated and the crude product was purified by column chromatography ($SiO_2$; *n*-hexane/MTBE 10:1 containing 5 vol% $NEt_3$) to afford **3** as a red, crystalline solid. Yield: 365 mg (1.46 mmol, 42%).[39] $^1$H NMR (400 MHz, 298 K, $CDCl_3$): $\delta$ = 1.28 (d, 12H, $^3J_{HH}$ = 6.3 Hz, $CH(CH_3)_2$), 3.91–4.00 (sept, 2H, $^3J_{HH}$ = 6.2 Hz, $CH(CH_3)2$), 6.23 (d, 2H, $^3J_{HH}$ = 12.0 Hz, 3 H, 7 H), 8.05 (d, 2H, $^3J_{HH}$ = 11.3 Hz, 4 H, 6 H) ppm.

**3,4–Bis(*iso*propylamino)benzaldehyde (4)**: $NaNO_2$ (750 mg, 10.9 mmol) was added to a solution of **2** (2.93 g, 10.4 mmol) in DMSO (40 mL). The mixture was stirred at 150 °C for 16 d, and extracted with a mixture of $H_2O$ (150 mL) and MTBE (150 mL). The work-up was performed as described above for **3**. Upon column chromatography, 3,4-bis(*iso*propylamino)benzaldehyde (**4**) was isolated as a brownish solid. Yield: 108 mg, 490 μmol (5%). $^1$H NMR (400 MHz, 298 K, $CDCl_3$): $\delta$ = 1.23 (d, 6H, $^3J_{HH}$ = 6.2 Hz, 3-NCH($CH_3$)$_2$), 1.29 (d, 6H, $^3J_{HH}$ = 6.2 Hz, 4-NCH($CH_3$)$_2$), 3.56–3.58 (sept, 1H, $^3J_{HH}$ = 6.2 Hz, 3-NC*H*($CH_3$)$_2$), 3.70–3.75 (sept, 1H, $^3J_{HH}$ = 6.3 Hz, 4-NC*H*($CH_3$)$_2$), 4.32 (br s, 2H, N*H*), 6.65 (d, 1H, $^3J_{HH}$ = 8.2 Hz, 5-H), 7.28 (s, 1H, 2-H), 7.36 (d, 1H, $^3J_{HH}$ = 7.9 Hz, 6-H), 9.71 (s, 1H, C*H*O) ppm. $^{13}$C{$^1$H} NMR (101 MHz, 298 K, [$D_5$]pyridine): $\delta$ = 22.97 (s, 4-NCH($CH_3$)$_2$), 23.07 (s, 3-NCH($CH_3$)$_2$), 44.16 (s, NCH($CH_3$)$_2$), 45.42 (s, NCH($CH_3$)$_2$), 109.26 (s, 5-*C*), 114.51 (s, 2-*C*), 126.66 (s, 3-*C*), 127.73 (s, 6-*C*), 133.97 (s, 1-*C*), 145.04 (s, 4-*C*), 190.99 (s, *C*HO) ppm. Elemental analysis calcd (%) for

 

$C_{13}H_{20}N_2O$ (220.32 g mol$^{-1}$): C 70.87, H 9.15, N 12.72; found: C 70.71, H 9.19, N 12.73.

**[Li(NO$_2$–ATI$^{iPr/iPr}$)] (5-Li)**: $LiCH_2SiMe_3$ (77.1 mg, 818 μmol) was added to a THF (6 mL) solution of **3** (200 mg, 802 μmol). The solvent was evaporated and the residual solid was washed with $Et_2O$ (3 mL) and *n*-pentane (3 x 3 mL), affording **5**-Li as an orange, crystalline solid. Yield: 66%, 145 mg, 528 μmol, contains 0.27 equiv. *n*-pentane, which could not be completely removed even after several hours of drying in vacuum. Single crystals suitable for X-ray diffraction analysis were obtained by diffusion of *n*-pentane (1 mL) into a solution of **5**-Li (9.0 mg) in pyridine (2 mL). $^1$H NMR (400 MHz, 298 K, [D$_5$]pyridine): $\delta = 0.95$ (d, 12H, $^3J_{HH} = 5.9$ Hz, CH(C*H*$_3$)$_2$), 3.88–3.94 (sept, 2H, $^3J_{HH} = 6.2$ Hz, C*H*(CH$_3$)$_2$), 6.22 (d, 2H, $^3J_{HH} = 12.6$ Hz, 3-H, 7-H), 8.50 (d, 2H, $^3J_{HH} = 12.6$ Hz, 4-H, 6-H) ppm. $^{13}$C{$^1$H} NMR (101 MHz, 298 K, [D$_5$]pyridine): $\delta = 23.90$ (s, CH(*C*H$_3$)$_2$), 50.29 (s, *C*H(CH$_3$)$_2$), 106.12 (s, 3-C, 7-C), 129.52 (s, 4-C, 6-C), 130.71 (s, 5-C), 164.30 (s, 1-C, 2-C) ppm. $^7$Li NMR (156 MHz, 298 K, [D$_5$]pyridine): $\delta =$ 2.99 (s) ppm. Elemental analysis calcd (%) for $C_{13}H_{18}LiN_3O_2{\cdot}C_5H_5N$ (334.20 g mol$^{-1}$): C 64.66, H 6.93, N 16.76; found: C 64.46, H 6.99, N 16.93.

**[Na(NO$_2$–ATI$^{iPr/iPr}$)] (5-Na)**: $NaN(SiMe_3)_2$ (69 mg, 373 μmol) was added to a THF (2 mL) solution of **5** (93 mg, 373 μmol). The solvent was evaporated, and the residual solid was washed with $Et_2O$ and *n*-pentane (3 x 3 mL, respectively), affording **5**-Na as an orange, crystalline solid. Yield: 79%, 83 mg, 296 μmol, containing 0.06 equiv. THF and $Et_2O$, respectively, which could not be completely removed even after several hours of drying in vacuum. Single crystals suitable for X-ray diffraction analysis were obtained by diffusion of *n*-pentane (1 mL) into a solution of **5**-Na (10.0 mg) in pyridine (2 mL). After 3 d in solution, in the $^1$H NMR spectrum two sets of signals for the *E*,*E* and the *E*,*Z* isomer, respectively, were detected in a 1.0:1.5 ratio. (*E*,*E*)-**5**-Na: $^1$H NMR (400 MHz, 298 K, [D$_5$] pyridine): $\delta = 1.15$ (d, 12H, $^3J_{HH} = 6.3$ Hz, CH(C*H*$_3$)$_2$), 3.92–3.95 (sept, 2H, $^3J_{HH} = 6.2$ Hz, C*H*(CH$_3$)$_2$), 6.08 (d, 2H, $^3J_{HH} = 12.6$ Hz, 3-H, 7-H), 8.34 (d, 2H, $^3J_{HH} = 12.7$ Hz, 4-H, 6-H) ppm. $^{13}$C{$^1$H} NMR (101 MHz, 298 K, [D$_5$]pyridine): $\delta = 24.16$ (s, CH(*C*H$_3$)$_2$), 51.16 (s, CH(*C*H$_3$)2), 109.14 (s, 3-C, 7-C), 124.19 (s, 5-C), 128.53 (s, 4-C, 6-C), 163.68 (s, 1-C, 2-C) ppm. (*E*,*Z*)-**5**-Na: $^1$H NMR (400 MHz, 298 K, [D$_5$]pyridine): $\delta = 1.22$ (d, 6H, $^3J_{HH} = 6.2$ Hz, 1-NCH(C*H*3)2), 1.37 (d, 6H, $^3J_{HH} = 6.2$ Hz, 2-NCH (C*H*$_3$)$_2$), 4.01–4.04 (sept, 1H, $^3J_{HH} = 6.1$ Hz, 1-NCH(C*H*$_3$)$_2$), 4.53–4.56 (sept, 1H, $^3J_{HH} = 6.4$ Hz, 2-NCH(C*H*$_3$)$_2$), 6.11 (d, 1H, 3JHH = 13.3 Hz, 7 H), 6.51 (d, 1H, 3JHH = 12.7 Hz, 3 H), 8.22 (m, 2H, 4 C, 6 C) ppm. $^{13}$C {$^1$H} NMR (101 MHz, 298 K, [D$_5$]pyridine): $\delta = 24.30$ (s, 1-NCH(*C*H$_3$)$_2$), 25.10 (s, 2-NCH(*C*H$_3$)$_2$), 51.27 (s, 1 *N*CH(CH$_3$)$_2$), 51.68 (s, 2-*N*CH(CH$_3$)$_2$), 111.64 (s, 7-C), 122.51 (s, 3-C), 124.43 (s, 5-C), 126.43 (s, 4-C/6-C), 128.76 (s, 4-C/6-C), 160.78 (s, 1-C), 162.92 (s, 2-C) ppm. Elemental analysis calcd (%) for $C_{13}H_{18}NaN_3O_2{\cdot}(C_5H_5N)$ (350.17 g mol$^{-1}$): C 61.70, H 6.62, N 15.99, gef.: C: 61.57, H 6.45, N 15.65.

**[K(NO$_2$–ATI$^{iPr/iPr}$)] (5-K)**: $KN(SiMe_3)_2$ (84.0 mg, 421 μmol) and THF (2 mL) were added to a THF (2 mL) solution of **3** (100 mg, 401 μmol). The solvent was evaporated, and the residual solid was washed with $Et_2O$ (2×2 mL) and *n*-pentane (3×2 mL), affording **5**-K as a brown-orange, crystalline solid. Single crystals suitable for X-ray diffraction analysis were obtained by diffusion of *n*-pentane (2 mL) into a solution of **5**-K in pyridine (4 mL). Yield: 75%, 91 mg 301 μmol, contains 0.21 equiv. *n*-pentane, which could not be completely removed even after several hours of drying in vacuum, but could be substituted for pyridine by re-recrystallisation from this solvent. After 3 d in solution, in the $^1$H NMR spectrum two sets of signals for the *E*,*E* and the *E*,*Z* isomer, respectively, were detected in a 1.0:1.6 ratio. (*E*,*E*)-**5**-K: $^1$H NMR (400 MHz, 298 K, [D$_5$]pyridine): $\delta = 1.16$ (d, 12H, $^3J_{HH} = 6.1$ Hz, CH(C*H*$_3$)$_2$), 3.91–4.00 (sept, 2H, $^3J_{HH} =$ 6.1 Hz, CH(CH$_3$)$_2$), 6.01 (d, 2H, $^3J_{HH} = 12.7$ Hz, 3-H, 7-H, overlaps with 7-H of the *E*,*Z* isomer), 8.34 (d, 1H, $^3J_{HH} = 12.6$ Hz, 4-H, 6-H) ppm. $^{13}$C {$^1$H} NMR (101 MHz, 298 K, [D$_5$]pyridine): $\delta = 24.26$ (s, CH(*C*H$_3$)$_2$), 51.34 (s, *C*H(CH$_3$)$_2$), 109.16 (s, 3-C, 7-C), 126.35 (s, 5-C), 128.40 (s, 4-C, 6-C), 163.76 (s, 1-C, 2-C) ppm. $^{15}$N-$^1$H HMBC NMR (50 MHz, 500 MHz, 298 K, [D$_5$]pyridine): $\delta = -53.9$ (s, 1-N, 2-N) ppm. (*E*,*Z*)-5-**K**: $^1$H NMR (400 MHz, 298 K, [D$_5$]pyridine): $\delta = 1.24$ (d, 6H, $^3J_{HH} = 6.1$ Hz, 1-NC*H* (CH$_3$)$_2$), 1.39 (d, 6H, $^3J_{HH} = 6.2$ Hz, 2-NCH(CH$_3$)$_2$), 4.00–4.07 (sept, 1H, $^3J_{HH} = 6.2$ Hz, 1-NC*H*(CH$_3$)$_2$), 4.56–4.62 (sept, 1H, $^3J_{HH} = 6.1$ Hz, 2-NC*H* (CH$_3$)$_2$), 6.02 (d, 1H, $^3J_{HH} = 13.1$ Hz, 7-H, overlaps with 3-H, 7-H of the *E*,*E* isomer), 6.46 (d, 1H, $^3J_{HH} = 13.0$ Hz, 3-H), 8.25 (d, 2H, $^3J_{HH} =$ 12.4 Hz, 4-H), 8.26 (d, 1H, $^3J_{HH} = 13.4$ Hz, 6-H) ppm. $^{13}$C{$^1$H} NMR (101 MHz, 298 K, [D$_5$]pyridine): $\delta = 24.37$ (s, 1 NCH(*C*H$_3$)$_2$), 25.14 (s, 2-NCH(*C*H$_3$)$_2$), 51.18 (s, 1-NCH(CH$_3$)$_2$), 51.57 (s, 2-NCH(CH$_3$)$_2$), 110.40 (s, 7-C), 121.52 (s, 3-C), 125.90 (s, 5-C), 126.59 (s, 4-C), 128.93 (s, 6-C), 160.82 (s, 1-C), 163.01 (s, 2-C) ppm. $^{15}$N,$^1$H HMBC NMR (50 MHz, 500 MHz, 298 K, [D$_5$]pyridine): $\delta = -41.2$ (s, 2-N), −32.6 (s, 1-N) ppm. Elemental analysis calcd (%) for $C_{13}H_{18}KN_3O_2{\cdot}C_5H_5N$ (366.15 g mol$^{-1}$): C 58.99, H 6.33, N 15.29; found: C 58.95, H 6.45, N 15.52.

**[Na(15-crown-5)(NO$_2$–ATI$^{iPr/iPr}$)] (6-Na)**: 15-crown-5 (19.2 mg, 87.2 μmol) was added to a THF (3 mL) suspension of **5**-Na (25.0 mg, 87.0 μmol). The resulting orange solution was layered with *n*-pentane and left standing for 6 d. The precipitate was isolated by filtration, washed with $Et_2O$ (2 mL) and pentane (3 x 2 mL) and dried in vacuum, affording **6**-Na as a yellow, crystalline solid. Yield: 85%, 37.6 mg, 74.3 μmol, contains trace amounts of *n*-pentane, which can be removed by prolonged exposure to reduced pressure. In the $^1$H NMR spectrum two sets of signals for the *E*,*E* and the *E*,*Z* isomer, respectively, were detected in a 1.0:1.9 ratio. (*E*,*E*)-**6**-Na: $^1$H NMR (400 MHz, 298 K, [D$_5$]pyridine): $\delta = 1.20$ (d, 12H, $^3J_{HH} = 6.6$ Hz, CH(C*H*$_3$)$_2$), 3.59 (s, 20H, 15-crown-5 C*H*$_2$), 3.93–3.99 (sept, 2H, $^3J_{HH} =$ 5.9 Hz, C*H*(CH$_3$)$_2$), 6.10 (d, 2H, $^3J_{HH} = 12.6$ Hz, 3-H, 7-H), 8.29 (d, 2H, $^3J_{HH} = 12.8$ Hz, 4-H, 6-H) ppm. $^{13}$C{$^1$H} NMR (125 MHz, 298 K, [D$_5$] pyridine): $\delta = 24.33$ (s, CH(*C*H$_3$)$_2$), 51.26 (s, *C*H(CH$_3$)$_2$), 69.78 (15-crown-5 *C*H$_2$), 109.59 (s, 3-C, 7-C), 126.11 (s, 5-C), 128.25 (s, 4-C, 6-C), 163.43 (s, 1-C, 2-C) ppm. $^{15}$N $^1$H HMBC NMR (50.7 MHz, 298 K, [D$_5$] pyridine): $\delta = -63.2$ (overlaps with [D$_5$]pyridine, 1-N, 2-N), −25.6 (s, NO$_2$) ppm. (*E*,*Z*)-**6**-Na: $^1$H NMR (400 MHz, 298 K, [D$_5$]pyridine): $\delta =$ 1.22 (d, 6H, $^3J_{HH} = 6.33$ Hz, 1-NCH(C*H*$_3$)$_2$), 1.37 (d, 6H, $^3J_{HH} = 6.21$ Hz, 2-NCH(C*H*$_3$)$_2$), 3.59 (s, 20H, 15-crown-5 C*H*$_2$), 3.99–4.05 (sept, 1H, $^3J_{HH} = 6.19$ Hz, 1-NC*H*(CH$_3$)$_2$), 4.52–4.58 (sept, 1H, $^3J_{HH} = 6.18$ Hz, 2-NC*H*(CH$_3$)$_2$), 6.06 (d, 1H, $^3J_{HH} = 12.8$ Hz, 7-H), 6.48 (d, 1H, $^3J_{HH} =$ 12.7 Hz, 3-H), 8.19 (dd, 1H, $^3J_{HH} = 5.03$ Hz, $^4J_{HH} = 1.88$, 6-H), 8.23 (dd, 1H, $^3J_{HH} = 5.03$ Hz, $^4J_{HH} = 1.88$, 4-H) ppm. $^{13}$C{$^1$H} NMR (101 MHz, 298 K, [D$_5$]pyridine): $\delta = 24.35$ (s, 1-NCH(*C*H$_3$)$_2$), 25.1 (s, 2-NCH(*C*H$_3$)$_2$), 51.20 (s, 1-*N*CH(CH$_3$)$_2$), 51.58 (s, 2 *N*CH(CH$_3$)$_2$), 69.78 (15-crown-5 *C*H$_2$), 110.58 (s, 7-C), 121.61 (s, 3-C), 125.40 (s, 5-C), 126.62 (s, 4-C), 128.93 (s, 6-C), 160.81 (s, 1-C), 162.97 (s, 2-C) ppm. $^{15}$N $^1$H HMBC NMR (50.7 MHz, 298 K, [D$_5$]pyridine): $\delta = -51.0$ (s, 2-N), −42.3 (s, 1-N), −31.6 (s, NO$_2$) ppm. $^{23}$Na NMR (106 MHz, 298 K, [D$_5$]pyridine): $\delta = 0.94$ (br s) ppm. Elemental analysis calcd (%) for $C_{23}H_{38}N_3NaO_7$ (491.56 g mol$^{-1}$): C 56.20, H 7.79, N 8.55; found: C 56.21, H 7.82, N 8.64.

**[K(18-crown-6)(NO$_2$–ATI$^{iPr/iPr}$)] (6-K)**: $KN(SiMe_3)_2$ (86 mg, 432 μmol) and 18-crown-6 (114 mg, 432 μmol) were added to a THF (3 mL) solution of **3** (108 mg, 432 μmol). The solvent was evaporated, and the residual solid was washed with *n*-pentane (4×15 mL), and dried in vacuum, affording **6**-K as a yellow, crystalline solid. Yield: 83%, 202 mg, 349 mmol, contains 0.19 equiv. THF, which can be removed by prolonged exposure of the sample to reduced pressure. In the $^1$H NMR spectrum two sets of signals for the *E*,*E* and the *E*,*Z* isomer, respectively, were detected in a 1.0:1.5 ratio. (*E*,*E*)-**6**-K: $^1$H NMR (400 MHz, 298 K, [D$_5$]pyridine): $\delta = 1.22$ (d, 12H, $^3J_{HH} =$ 6.2 Hz, CH(C*H*$_3$)$_2$), 1.61–1.64 (m, *n*×4H, β-THF), 3.47 (s, 24H, 18-crown-6 C*H*2), 3.65-3.67 (m, *n*×4H, α-THF), 3.98–4.12 (br sept, 2H, $^3J_{HH} = 6.2$ Hz, C*H*(CH$_3$)$_2$, overlaps with C*H*(CH3)$_2$ of the *E*,*Z* isomer), 6.04 (br d, 2H, $^3J_{HH} = 12.7$ Hz, 3-H, 7-H), 8.37-8.44 (m, 2H, 4-H, 6-H, overlaps with 4-H and 6-H of the *E*,*Z* isomer) ppm. $^{13}$C{$^1$H} NMR

 

(101 MHz, 298 K, [D$_5$]pyridine): $\delta$ = 24.49 (s, CH($CH_3$)$_2$), 26.27 (s, β-THF), 50.98 (s, $CH$(CH$_3$)$_2$), 68.30 (s, α-THF), 70.78 (18-crown-6 $CH$2), 108.14 (s, 3-C, 7-C), 126.00 (s, 5-C), 127.22 (s, 4-C, 6-C), 163.44 (s, 1-C, 2-C) ppm. (*E*,*Z*)-6-**K**: $^1$H NMR (400 MHz, 298 K, [D$_5$]pyridine): $\delta$ = 1.26 (d, 6H, $^3J_{HH}$ = 6.2 Hz, 1-NCH(C$H_3$)$_2$), 1.39 (d, 6H, $^3J_{HH}$ = 6.2 Hz, 2-NCH(C$H_3$)$_2$), 1.61–1.64 (m, *n* ×4H, β-THF), 3.47 (s, 24H, 18-crown-6 C$H_2$), 3.65–3.67 (m, *n* ×4H, α-THF), 3.98–4.12 (br sept, 2H, $^3J_{HH}$ = 6.2 Hz, 1-NC$H$(CH$_3$)$_2$, overlaps with $CH$(CH$_3$)$_2$ of the *E*,*E* isomer), 4.61–4.71 (sept, 1H, $^3J_{HH}$ = 6.2 Hz, 2-NC$H$(CH$_3$)$_2$), 5.97 (d, 1H, $^3J_{HH}$ = 12.5 Hz, 7-H), 6.45 (d, 1H, $^3J_{HH}$ = 12.6 Hz, 3-H), 8.37–8.44 (m, 2H, 4-H, 6-H, overlaps with 4-H and 6-H of the *E*,*E* isomer) ppm. $^{13}$C{$^1$H} NMR (101 MHz, 298 K, [D$_5$]pyridine): $\delta$ = 24.60 (s, 1-NCH(C$H_3$)$_2$), 25.20 (s, 2-NCH(C$H_3$)$_2$), 26.27 (s, β-THF), 51.30 (s, 1-N$C$H(CH$_3$)$_2$), 51.33 (s, 2-N$C$H(CH$_3$)$_2$), 68.30 (s, α-THF), 70.78 (18-crown-6 $C$H$_2$), 107.30 (s, 7-C), 119.06 (s, 3-C), 125.83 (s, 5-C), 128.33 (s, 4-C/6-C), 129.55 (s, 4-C/6-C), 160.97 (s, 1-C), 163.19 (s, 2-C) ppm. Elemental analysis calcd (%) for $C_{25}H_{42}KN_3O_8$ (551.72 g mol$^{-1}$): C 54.43, H 7.67, N 7.62; found: C 54.84, H 7.76, N 7.85.

**[Na(12-crown-4)$_2$][(NO$_2$–ATI$^{iPr/iPr}$)] (7)**: 12-crown-4 (129 mg, 738 μmol) was added to a THF (3 mL) suspension of **5**-Na (100 mg, 369 μmol). The solvent was evaporated, and the residual solid was washed with *n*-pentane (3×2 mL), and dried in vacuum to afford **7** as a yellow solid. Yield: 90%, 209 mg, 333 μmol, contains 0.05 equiv. THF. In the $^1$H NMR spectrum two sets of signals for the *E*,*E* and the *E*,*Z* isomer, respectively, were detected in a 1.0:1.3 ratio. (*E*,*E*)-**7**: $^1$H NMR (400 MHz, 298 K, [D$_5$]pyridine): $\delta$ = 1.22 (d, 12H, $^3J_{HH}$ = 6.2 Hz, CH(C$H_3$)$_2$), 3.61 (s, 32H, 12-crown-4 C$H_2$), 3.94–4.00 (br sept, 2H, C$H$(CH$_3$)$_2$), 6.06 (d, 2H, $^3J_{HH}$ = 12.7 Hz, 3-H,7-H), 8.41 (d, 2H, $^3J_{HH}$ = 12.6 Hz, 4-H, 6-H) ppm. $^{13}$C{$^1$H} NMR (101 MHz, 298 K, [D$_5$] pyridine): $\delta$ = 22.95 (s, CH($CH_3$)$_2$), 51.12 (s, $CH$(CH$_3$)$_2$), 68.30 (12-crown-4 $CH_2$), 107.67 (s, 3-C, 7-C), 125.75 (s, 5-C), 128.79 (s, 4-C, 6-C), 163.65 (s, 1-C, 2-C) ppm. (*E*,*Z*)-**7**: $^1$H NMR (400 MHz, 298 K, [D$_5$] pyridine): $\delta$ = 1.24 (d, 6H, $^3J_{HH}$ = 6.2 Hz, 1-NCH(C$H_3$)$_2$), 1.38 (d, 6H, $^3J_{HH}$ = 6.2 Hz, 2-NCH(C$H_3$)$_2$), 3.61 (s, 32H, 12-crown-4 C$H_2$), 4.01–4.10 (sept, 1H, $^3J_{HH}$ = 6.2 Hz, 1-NC$H$(CH$_3$)2), 4.56–4.65 (sept, 1H, $^3J_{HH}$ = 6.2 Hz, 2-NC$H$(CH$_3$)$_2$), 6.04 (d, 1H, $^3J_{HH}$ = 12.7 Hz, 7-H), 6.47 (d, 1H, $^3J_{HH}$ = 12.9 Hz, 3-H), 8.32 (ddd, 1H, $^3J_{HH}$ = 12.9 Hz, $^4J_{HH}$ = 2.0, 4-H), 8.34 (dd, 1H, $^3J_{HH}$ = 12.8 Hz, $^4J_{HH}$ = 1.9, 6-H) ppm. $^{13}$C{$^1$H} NMR (101 MHz, 298 K, [D$_5$]pyridine): $\delta$ = 24.40 (s, 1-NCH(C$H_3$)$_2$), 25.15 (s, 2-NCH(C$H_3$)$_2$), 51.15 (s, 1 NCH(CH$_3$)$_2$), 51.46 (s, 2 NCH(CH$_3$)$_2$), 68.30 (12-crown-4 $CH_2$), 109.37 (s, 7-C), 120.69 (s, 3-C), 125.75 (s, 5-C), 126.85 (s, 4-C), 129.19 (s, 6-C), 160.88 (s, 1-C), 163.07 (s, 1-C) ppm. $^{23}$Na NMR (106 MHz, 298 K, [D$_5$]pyridine): $\delta$ = 1.7 (br s, Na) ppm. Elemental analysis calcd (%) for $C_{29}H_{50}N_3NaO_{10}$ (623.72 g mol$^{-1}$): C 55.85, H 8.08, N 6.74; found: C 56.00, H 8.25, N 6.85.

**[Ag(NO$_2$–ATI$^{iPr/iPr}$)] (8)**: Ag[BF$_4$] (7 mg, 36 μmol) was added to a suspension of [**5**-Na(thf)$_{0.06}$(Et$_2$O)$_{0.06}$] (10 mg, 36 μmol) in pyridine (1 mL). The red suspension was left at room temperature for 1 h without stirring and layered with Et$_2$O (1 mL). After 2 d, the resulting red crystals of **8** were isolated by filtration and dried in vacuum. Yield: 1 mg. The isolated solid contains significant amounts of NaBF$_4$ according to $^{19}$F and $^{11}$B NMR spectroscopy. The batch analysed NMR-spectroscopically contained n = 0.36 equiv. Et$_2$O. $^1$H NMR (400 MHz, 298 K, [D$_5$]pyridine): $\delta$ = 1.12–1.16 (t, *n*×3H, Et$_2$O), 1.25 (d, 12H, $^3J_{HH}$ = 6.2 Hz, CH(C$H_3$)$_2$), 3.34–3.39 (q, *n*×4H, Et$_2$O), 3.91–4.00 (sept, 4H, $^3J_{HH}$ = 6.2 Hz, CH(C$H_3$)$_2$), 6.03 (d, 2H, $^3J_{HH}$ = 12.9 Hz, 3-H, 7-H), 8.38 (d, 2H, $^3J_{HH}$ = 12.8 Hz, 4-H, 6-H) ppm. $^{13}$C{$^1$H} NMR (101 MHz, 298 K, [D$_5$]pyridine): $\delta$ = 15.96 (s, Et$_2$O), 24.96 (s, CH($CH_3$)$_2$), 51.02 (s, $CH$(CH$_3$)$_2$), 66.23 (s, Et$_2$O), 106.66 (s, 3-C, 7-C), 128.86 (s, 5-C), 129.78 (s, 4-C, 6-C), 162.23 (s, 1-C, 2-C) ppm.

**[Na(15-crown-5)Ag(NO$_2$–ATI$^{iPr/iPr}$)$_2$] (9)**: Ag[BF$_4$] (7.2 mg, 37 μmol) and **6**-Na (18 mg, 37 μmol) were added to a [D$_5$]pyridine (0.5 mL) suspension of **5**-Na (10 mg, 37 μmol). The resulting solution was layered with Et$_2$O (0.5 mL). After 3 d, red crystals of **10** were isolated by filtration and dried in vacuum. Yield: 87%, 15 mg, 16.2 μmol, contains 1 equiv. pyridine.[40] $^1$H NMR (400 MHz, 298 K, [D$_5$]pyridine): $\delta$ = 1.26 (d, 24H, $^3J_{HH}$ = 6.1 Hz, CH(C$H_3$)$_2$), 3.59 (s, 20H, 12-crown-4 C$H_2$), 3.91–4.00 (sept, 4H, $^3J_{HH}$ = 6.2 Hz, CH(CH$_3$)$_2$), 6.02 (d, 4H, $^3J_{HH}$ = 12.5 Hz, 3-H, 7-H), 8.41 (d, 4H, $^3J_{HH}$ = 12.8 Hz, 4-H, 6-H) ppm. $^{13}$C{$^1$H} NMR (101 MHz, 298 K, [D$_5$]pyridine): $\delta$ = 25.00 (s, CH($CH_3$)$_2$), 51.02 (s, $CH$(CH$_3$)$_2$), 69.35 (s, 12-corwn-4 $CH_2$), 106.18 (s, 3-C, 7-C), 129.05 (s, 5-C), 129.75 (s, 4-C, 6-C), 162.18 (s, 1-C, 2-C) ppm. Elemental analysis calcd (%) for $C_{36}H_{56}AgN_6NaO_9{\cdot}C_5H_5N$ (926.84 g mol$^{-1}$): C 53.13, H 6.63, N 10.58; found: C 53.33, H 6.73, N 10.75.

**[Na(12-crown-4)$_2$][Ag(NO$_2$–ATI$^{iPr/iPr}$)$_2$] (10)**: Ag[BF$_4$] (1.6 mg, 8.0 μmol) was added to a THF (1 mL) solution of **7** (10 mg, 15 μmol) After 2 h at RT, the red solution was layered with *n*-hexane (2 mL). After 1 d, the resulting red crystals were isolated by filtration. The filtrate was layered with additional *n*-hexane (2 mL), and the resulting second crop of crystals was isolated by filtration. Both batches were combined and recrystallised from THF/Et$_2$O (1:2). Yield: 4.2 mg. The amount of [Na(12-crown-4)$_2$][BF$_4$] was determined to be 0.9 mol% using quantitative $^{19}$F NMR spectroscopy by dissolving the isolated compound and K[BF(CN)$_3$] as the internal standard in [D$_5$]pyridine (0.5 mL). $^1$H NMR (400 MHz, 298 K, [D$_5$] pyridine): $\delta$ = 0.81 (t, *n*-pentane), 1.26 (d, 24H, $^3J_{HH}$ = 6.2 Hz, CH-(C$H_3$)$_2$, overlaps with *n*-pentane), 3.60 (s, 32H, 12-crown-4 C$H_2$), 3.91–4.00 (sept, 4H, $^3J_{HH}$ = 6.2 Hz, C$H$(CH$_3$)$_2$), 6.02 (d, 4H, $^3J_{HH}$ = 12.8 Hz, 3-H, 7-H), 8.42 (d, 4H, $^3J_{HH}$ = 12.8 Hz, 4-H, 6-H) ppm. $^{13}$C{$^1$H} NMR (101 MHz, 298 K, [D$_5$]pyridine): $\delta$ = 14.61 (s, *n*-pentane), 22.96 (s, *n*-pentane), 24.99 (s, CH($CH_3$)$_2$), 51.00 (s, $CH$(CH$_3$)$_2$), 67.77 (s, 12-crown-4 $CH_2$), 106.15 (s, 3-C, 7-C), 129.76 (s, 5-C, overlaps with 4-C, 6-C), 129.76 (s, 4-C, 6-C), 162.19 (s, 1-C, 2-C) ppm. Elemental analysis calcd (%) for $C_{42}H_{68}AgN_6NaO_{12}$ (979.89 g mol$^{-1}$): C 51.48, H 7.00, N 8.58; found: C 51.89, H 7.02, N 8.74.

**[Na(12-crown-4)$_2$][(3-Ph$_3$C–5-NO$_2$–ATI$^{iPr/iPr}$)] (11)**: Ph$_3$CCl (9 mg, 32 μmol) and NaH (1 mg, 32 μmol) were added to a THF (1 mL) solution of **7** (20 mg, 32 μmol). The solution was stirred for 48 h at RT, filtered, and the solvent was evaporated. The residual orange solid was washed with Et$_2$O (3×5 mL) and dried in vacuum. Yield: 18%, 5 mg, 6 μmol, contains n = 0.38 equiv. Et$_2$O and m = 0.2 equiv. *n*-pentane, which can be removed by prolonged exposure to reduced pressure. $^1$H NMR (400 MHz, 298 K, [D$_8$]THF): $\delta$ = 0.62 (d, 6H, $^3J_{HH}$ = 5.6 Hz, 2-NCH(C$H_3$)$_2$), 0.88 (t, m ×6H, *n*-pentane), 1.10 (t, *n* ×6H, Et$_2$O), 1.12 (d, 6H, $^3J_{HH}$ = 6.1 Hz, 1-NCH(C$H_3$)$_2$), 1.32 (m, *n*-pentane), 3.35–3.40 (q, n ×4H, Et$_2$O), 3.58 (s, 32H, 12-crown-4 C$H_2$), 3.59–3.68 (m, 1H, 2-NC$H$(CH$_3$)$_2$, overlaps with crown ether signal), 3.85–3.94 (sept, 1H, $^3J_{HH}$ = 6.2 Hz, 1-NC$H$(CH$_3$)$_2$), 5.81 (d, 1H, $^3J_{HH}$ = 12.2 Hz, 7-H), 6.94–6.98 (m, 3H, p-Ph), 7.03-7.06 (m, 6H, m-Ph), 7.22 (d, 1H, $^4J_{HH}$ = 1.6 Hz, 4-H), 7.41-7.43 (m, 6H, o-Ph), 7.61 (dd, 1H, $^3J_{HH}$ = 12.1 Hz, $^4J_{HH}$ = 1.5 Hz, 6-H) ppm. $^{13}$C{$^1$H} NMR (101 MHz, 298 K, [D$_8$] THF): $\delta$ = 14.16 (s, *n*-pentane), 15.48 (s, Et$_2$O), 23.00 (s, *n*-pentane), 23.37 (s, 2-NCH(C$H_3$)$_2$), 24.08 (s, 1-NCH(C$H_3$)$_2$), 34.87 (s, *n*-pentane), 50.95 (s, 1-N$C$H(CH$_3$)$_2$), 51.14 (s, 2-N$C$H(CH$_3$)$_2$), 66.13 (s, Et$_2$O), 70.33 (s, 12-crown-4 $CH_2$), 107.79 (s, 7-C), 124.20 (s, 5-C), 125.07 (s, p-Ph), 127.06 (s, m-Ph), 128.92 (s, 6-C), 130.81 (s, 4-C), 132.46 (s, o-Ph), 134.59 (s, 3-C), 136.28 (s, $C$Ph$_3$), 149.64 (s, *i*-Ph), 160.38 (s, 1-C), 163.62 (s, 2-C) ppm. Elemental analysis calcd (%) for $C_{48}H_{64}N_3NaO_{10}$ (866.04 g mol$^{-1}$): C 66.57, H 7.45, N 4.85; found: C 66.33, H 7.64, N 4.86.

**[Na(Ph$_3$C–ATI$^{iPr/iPr}$)] (12)**: Ph$_3$CCl (41 mg, 147 μmol) and NaHMDS (54 mg, 294 μmol) were added to a THF (1 mL) solution of **1** (30 mg, 147 μmol). The solution was stirred for 2 h at RT, and the solvent was evaporated. The crude product was re-crystallised from THF/*n*-pentane (1:2.4 mL) at −30 °C. Yield: 73%, 61 mg, 107 μmol, contains *n* = 2 equiv. THF), 73%. $^1$H NMR (400 MHz, 298 K, [D$_8$]THF): $\delta$ = 1.08 (d, 12H, $^3J_{HH}$ = 6.2 Hz, CH(C$H_3$)$_2$), 1.72–1.79 (m, *n* ×4H, β-THF), 3.60–3.64 (m, *n* ×4H, α-THF), 3.64-3.71 (sept, 2H, $^3J_{HH}$ = 6.2 Hz, C$H$(CH$_3$)$_2$), 5.69 (d, 2H, $^3J_{HH}$ = 12.2 Hz, 3-H, 7-H), 6.33 (d, 2H, $^3J_{HH}$ = 12.2 Hz, 4-H, 6-H), 7.01–7.05 (m, 3H, *p*-Ph), 7.11–7.15 (m, 6H, *m*-Ph),

 

7.27-7.29 (m, 6H, *o*-Ph) ppm. $^{13}C\{^1H\}$ NMR (101 MHz, 298 K, [$D_8$]THF): $\delta$ = 24.49 (s, CH($CH_3$)$_2$), 26.19 (s, β-THF), 48.64 (s, $CH(CH_3)_2$), 68.02 (s, α-THF), 104.40 (s, 3-C, 7-C), 123.01 (s, 5-C), 125.38 (s, *p*-Ph), 127.37 (s, *m*-Ph), 132.02 (s, *o*-Ph), 135.66 (s, 4-C, 6-C), 149.85 (s, *i*-Ph), 161.99 (s, 1-C, 2-C) ppm. Elemental analysis calcd (%) for $C_{32}H_{33}N_2Na\cdot(C_4H_8O)_2$ (612.83 g mol$^{-1}$): C 78.40, H 8.06, N 4.57; found: C 78.42, H 7.97, N 4.71.

## *Acknowledgements*

Funding through the Fonds der Chemischen Industrie (FCI) and the Deutsche Forschungsgemeinschaft (DFG, LI 2860/3-1, LI 2860/5-1) is gratefully acknowledged. C.L. thanks Prof. Holger Braunschweig for continued support. Open Access funding enabled and organized by Projekt DEAL.

## Conflict of Interest

The authors declare no conflict of interest.

**Keywords:** aminotroponiminates · alkali metal · electrophilic substitution · isomerisation · non-coordinate anionic ligand

[1] F. T. Edelmann, *Chem. Soc. Rev.* **2009**, *38*, 2253–2268.
[2] a) K. G. Caulton, *Eur. J. Inorg. Chem.* **2012**, *2012*, 435–443; b) E. N. Nikolaevskaya, N. O. Druzhkov, M. A. Syroeshkin, M. P. Egorov, *Coord. Chem. Rev.* **2020**, *417*, 213353; c) F. J. de Zwart, B. Reus, A. A. H. Laporte, V. Sinha, B. de Bruin, *Inorg. Chem.* **2021**, *60*, 3274–3281.
[3] a) M. M. Khusniyarov, T. Weyhermüller, E. Bill, K. Wieghardt, *J. Am. Chem. Soc.* **2009**, *131*, 1208–1221; b) M. Ghosh, S. Sproules, T. Weyhermüller, K. Wieghardt, *Inorg. Chem.* **2008**, *47*, 5963–5970; c) N. Muresan, C. C. Lu, M. Ghosh, J. C. Peters, M. Abe, L. M. Henling, T. Weyhermüller, E. Bill, K. Wieghardt, *Inorg. Chem.* **2008**, *47*, 4579–4590.
[4] a) R. L. Webster, *Dalton Trans.* **2017**, *46*, 4483–4498; b) J. Spielmann, S. Harder, *Chem. Eur. J.* **2007**, *13*, 8928–8938.
[5] a) P. W. Roesky, *Chem. Soc. Rev.* **2000**, *29*, 335–345; b) A. Hanft, C. Lichtenberg, *Eur. J. Inorg. Chem.* **2018**, *2018*, 3361–3373.
[6] a) V. Lyaskovskyy, B. de Bruin, *ACS Catal.* **2012**, *2*, 270–279; b) V. K. K. Praneeth, M. R. Ringenberg, T. R. Ward, *Angew. Chem. Int. Ed.* **2012**, *51*, 10228–10234, *Angew. Chem.* **2012**, *124*, 10374–10380; c) O. R. Luca, R. H. Crabtree, *Chem. Soc. Rev.* **2013**, *42*, 1440–1459; d) W. Huang, P. L. Diaconescu, *Inorg. Chem.* **2016**, *55*, 10013–10023; e) D. L. J. Broere, R. Plessius, J. I. van der Vlugt, *Chem. Soc. Rev.* **2015**, *44*, 6886–6915; f) J. Jacquet, M. Desage-El Murr, L. Fensterbank, *ChemCatChem* **2016**, *8*, 3310–3316; g) W. Kaim, *Eur. J. Inorg. Chem.* **2012**, *2012*, 343–348; h) W. Kaim, *Inorg. Chem.* **2011**, *50*, 9752–9765; i) L. A. Berben, *Chem. Eur. J.* **2015**, *21*, 2734–2742; j) J. I. van der Vlugt, *Chem. Eur. J.* **2019**, *25*, 2651–2662.
[7] a) S. P. Green, C. Jones, A. Stasch, *Science* **2007**, *318*, 1754; b) C. Cui, H. W. Roesky, H.-G. Schmidt, M. Noltemeyer, H. Hao, F. Cimpoesu, *Angew. Chem. Int. Ed.* **2000**, *39*, 4274–4276; *Angew. Chem.* **2000**, *112*, 4444–4446.
[8] C. Lichtenberg, L. Viciu, M. Vogt, R. E. Rodríguez-Lugo, M. Adelhardt, J. Sutter, M. M. Khusniyarov, K. Meyer, B. de Bruin, E. Bill, H. Grützmacher, *Chem. Commun.* **2015**, *51*, 13890–13893.
[9] a) B. Rösch, T. X. Gentner, J. Langer, C. Färber, J. Eyselein, L. Zhao, C. Ding, G. Frenking, S. Harder, *Science* **2021**, *371*, 1125; b) J. Spielmann, F. Buch, S. Harder, *Angew. Chem. Int. Ed.* **2008**, *47*, 9434–9438; *Angew. Chem.* **2008**, *120*, 9576–9580; c) S. F. McWilliams, P. L. Holland, *Acc. Chem. Res.* **2015**, *48*, 2059–2065.
[10] a) A. Zulys, M. Dochnahl, D. Hollmann, K. Löhnwitz, J.-S. Herrmann, P. W. Roesky, S. Blechert, *Angew. Chem. Int. Ed.* **2005**, *44*, 7794–7798; *Angew. Chem.* **2005**, *117*, 7972–7976; b) C. Lichtenberg, M. Adelhardt, T. L. Gianetti, K. Meyer, B. de Bruin, H. Grützmacher, *ACS Catal.* **2015**, *5*, 6230–6240; c) C. Lichtenberg, L. Viciu, M. Adelhardt, J. Sutter, K. Meyer, B. de Bruin, H. Grützmacher, *Angew. Chem. Int. Ed.* **2015**, *54*, 5766–5771, *Angew. Chem.* **2015**, *127*, 5858–5863; d) R. E. Cowley, N. A. Eckert, J. Elhaïk, P. L. Holland, *Chem. Commun.* **2009**, 1760–1762.
[11] a) H. V. R. Dias, Z. Wang, W. Jin, *Coord. Chem. Rev.* **1998**, *176*, 67–86; b) J. J. Drysdale, W. W. Gilbert, H. K. Sinclair, W. H. Sharkey, *J. Am. Chem. Soc.* **1958**, *80*, 3672–3675; c) W. R. Brasen, H. E. Holmquist, R. E. Benson, *J. Am. Chem. Soc.* **1960**, *82*, 995–996; d) R. M. Claramunt, D. Sanz, M. Pérez-Torralba, E. Pinilla, M. R. Torres, J. Elguero, *Eur. J. Org. Chem.* **2004**, *2004*, 4452–4466; e) M. Dochnahl, K. Löhnwitz, J.-W. Pissarek, M. Biyikal, S. R. Schulz, S. Schön, N. Meyer, P. W. Roesky, S. Blechert, *Chem. Eur. J.* **2007**, *13*, 6654–6666; f) E. Szuromi, J. Klosin, K. A. Abboud, *Organometallics* **2011**, *30*, 4589–4597; g) P. W. Roesky, *J. Organomet. Chem.* **2001**, *621*, 277–283; h) A. Hanft, C. Lichtenberg, *Dalton Trans.* **2018**, *47*, 10578–10589.
[12] a) M. Dochnahl, K. Löhnwitz, A. Lühl, J.-W. Pissarek, M. Biyikal, P. W. Roesky, S. Blechert, *Organometallics* **2010**, *29*, 2637–2645; b) J. Jenter, A. Lühl, P. W. Roesky, S. Blechert, *J. Organomet. Chem.* **2011**, *696*, 406–418; c) W. R. Brasen, H. E. Holmquist, R. E. Benson, *J. Am. Chem. Soc.* **1961**, *83*, 3125–3135; d) W. F. Richter, K. Hartke, W. Massa, G. Münninghoff, *Chem. Ber.* **1989**, *122*, 1133–1137; e) M. Dochnahl, K. Löhnwitz, J.-W. Pissarek, P. W. Roesky, S. Blechert, *Dalton Trans.* **2008**, 2844; f) K. Löhnwitz, M. J. Molski, A. Lühl, P. W. Roesky, M. Dochnahl, S. Blechert, *Eur. J. Inorg. Chem.* **2009**, *2009*, 1369–1375; g) D. R. Eaton, A. D. Josey, R. E. Benson, W. D. Phillips, T. L. Cairns, *J. Am. Chem. Soc.* **1962**, *84*, 4100–4106.
[13] a) C. Lichtenberg, *Organometallics* **2016**, *35*, 894–902; b) A. Hanft, C. Lichtenberg, *Organometallics* **2018**, *37*, 1781–1787; c) A. Hanft, M. Jürgensen, R. Bertermann, C. Lichtenberg, *ChemCatChem* **2018**, *10*, 4018–4027.
[14] a) A. V. Korolev, F. Delpech, S. Dagorne, I. A. Guzei, R. F. Jordan, *Organometallics* **2001**, *20*, 3367–3369; b) F. Delpech, I. A. Guzei, R. F. Jordan, *Organometallics* **2002**, *21*, 1167–1176; c) V. Kirin, P. W. Roesky, *Z. Anorg. Allg. Chem.* **2004**, *630*, 466–469.
[15] a) C. Lichtenberg, I. Krummenacher, *Chem. Commun.* **2016**, *52*, 10044–10047; b) A. Hanft, I. Krummenacher, C. Lichtenberg, *Chem. Eur. J.* **2019**, *25*, 11883–11891.
[16] K. J. Franz, S. J. Lippard, *J. Am. Chem. Soc.* **1999**, *121*, 10504–10512.
[17] a) P. L. Pauson, *Chem. Rev.* **1955**, *55*, 9–136; b) T. Mukai, *Bull. Chem. Soc. Jpn.* **1959**, *32*, 272–279; c) T. Toda, *Bull. Chem. Soc. Jpn.* **1967**, *40*, 588–590; d) G. Biggi, A. J. De Hoog, F. Del Cima, F. Pietra, *J. Am. Chem. Soc.* **1973**, *95*, 7108–7113; e) M. Biyikal, K. Löhnwitz, P. W. Roesky, S. Blechert, *Synlett* **2008**, *2008*, 3106–3110; f) L. Hussein, N. Purkait, M. Biyikal, E. Tausch, P. W. Roesky, S. Blechert, *Chem. Commun.* **2014**, *50*, 3862–3864; g) B. E. Klamm, C. J. Windorff, C. Celis-Barros, M. L. Marsh, T. E. Albrecht-Schmitt, *Inorg. Chem.* **2020**, *59*, 23–31; h) A. Hanft, M. Jürgensen, L. Wolz, K. Radacki, C. Lichtenberg, *Inorg. Chem.* **2020**, *59*, 17678–17688.
[18] H. V. R. Dias, W. Jin, R. E. Ratcliff, *Inorg. Chem.* **1995**, *34*, 6100–6105.
[19] F. H. Allen, O. Kennard, D. G. Watson, L. Brammer, A. G. Orpen, R. Taylor, *J. Chem. Soc. Perkin Trans. 2* **1987**, S1-S19.
[20] A. Domenicano, G. Schultz, I. Hargittai, M. Colapietro, G. Portalone, P. George, C. W. Bock, *Struct. Chem.* **1990**, *1*, 107–122.
[21] a) A. Ariza-Castolo, J. A. Montalvo-González, R. Montalvo-González, *Magn. Reson. Chem.* **2005**, *43*, 975–978; b) V. A. Semenov, D. O. Samultsev, A. Y. Rulev, L. B. Krivdin, *Magn. Reson. Chem.* **2015**, *53*, 1031–1034.
[22] a) R. Paetzold, M. Reichenbächer, K. Appenroth, *Z. Chem.* **1981**, *21*, 421–430; b) J. Gálvez, A. Guirado, *J. Comput. Chem.* **2010**, *31*, 520–531.
[23] a) A. E. Ayers, H. V. R. Dias, *Inorg. Chem.* **2002**, *41*, 3259–3268; b) S. Datta, P. W. Roesky, S. Blechert, *Organometallics* **2007**, *26*, 4392–4394; c) R. K. Siwatch, S. Kundu, D. Kumar, S. Nagendran, *Organometallics* **2011**, *30*, 1998–2005; d) S. Sinhababu, R. K. Siwatch, G. Mukherjee, G. Rajaraman, S. Nagendran, *Inorg. Chem.* **2012**, *51*, 9240–9248.
[24] a) S. Harder, *Chem. Eur. J.* **1999**, *5*, 1852–1861; b) M. L. Cole, C. Jones, P. C. Junk, *J. Chem. Soc. Dalton Trans.* **2002**, 896–905; c) A. Jaenschke, J. Paap, U. Behrens, *Organometallics* **2003**, *22*, 1167–1169.
[25] a) T. B. Marder, I. D. Williams, *J. Chem. Soc. Chem. Commun.* **1987**, 1478–1480; b) G. Boche, B. Ledig, M. Marsch, K. Harms, *Acta Crystallogr. Sect. E Struct. Rep. Online* **2001**, *57*, m570-m572.
[26] A. Hanft, K. Radacki, C. Lichtenberg, *Chem. Eur. J.* **2021**, *27*, 6230–6239.
[27] R. G. Pearson, *J. Chem. Educ.* **1968**, *45*, 581.
[28] a) J. A. Flores, K. Pal, M. E. Carroll, M. Pink, J. A. Karty, D. J. Mindiola, K. G. Caulton, *Organometallics* **2014**, *33*, 1544–1552; b) S. Durini, G. A. Ardizzoia, B. Therrien, S. Brenna, *New J. Chem.* **2017**, *41*, 3006–3014.
[29] a) H.-Y. Liu, H. Wu, J.-F. Ma, *Acta Crystallogr. Sect. E Struct. Rep. Online* **2006**, *62*, m325–m326; b) S. K. Emashova, A. A. Titov, O. A. Filippov, A. F.

 

Smol'yakov, E. M. Titova, L. M. Epstein, E. S. Shubina, *Eur. J. Inorg. Chem.* **2019**, *2019*, 4855–4861.
[30] a) H. V. R. Dias, S. Singh, *Inorg. Chem.* **2004**, *43*, 7396–7402; b) C. Shimokawa, S. Itoh, *Inorg. Chem.* **2005**, *44*, 3010–3012; c) H. A. Chiong, O. Daugulis, *Organometallics* **2006**, *25*, 4054–4057.
[31] a) S. W. Jaros, U. Śliwińska-Hill, A. Białońska, D. S. Nesterov, P. Kuropka, J. Sokolnicki, B. Bażanów, P. Smoleński, *Dalton Trans.* **2019**, *48*, 11235–11249; b) O. Mamula, A. von Zelewsky, T. Bark, H. Stoeckli-Evans, A. Neels, G. Bernardinelli, *Chem. Eur. J.* **2000**, *6*, 3575–3585.
[32] a) H. V. R. Dias, Z. Wang, *Inorg. Chem.* **2000**, *39*, 3890–3893; b) H. V. R. Dias, A. E. Ayers, *Polyhedron* **2002**, *21*, 611–618.
[33] D. Yadav, R. K. Siwatch, G. Mukherjee, G. Rajaraman, S. Nagendran, *Inorg. Chem.* **2014**, *53*, 10054–10059.
[34] A. V. Korolev, E. Ihara, I. A. Guzei, V. G. Young, R. F. Jordan, *J. Am. Chem. Soc.* **2001**, *123*, 8291–8309.
[35] P. C. Hariharan, J. A. Pople, *Theor. Chim. Acta* **1973**, *28*, 213–222.
[36] R. Krishnan, J. S. Binkley, R. Seeger, J. A. Pople, *J. Chem. Phys.* **1980**, *72*, 650–654.
[37] A. D. Becke, *J. Chem. Phys.* **1993**, *98*, 5648–5652.
[38] a) S. Grimme, J. Antony, S. Ehrlich, H. Krieg, *J. Chem. Phys.* **2010**, *132*, 154104; b) J. Tomasi, B. Mennucci, R. Cammi, *Chem. Rev.* **2005**, *105*, 2999–3094.
[39] Varying yields were obtained in these reactions (see Supporting Informatiom).
[40] Data obtained from XRD and elemental analyses indicate the presence of 1 equiv. pyridine. Traces of [Na(15-crown-5)][$BF_4$] could be identified by $^{19}F\{^1H\}$ NMR spectroscopy.

Manuscript received: June 28, 2021
Accepted manuscript online: July 27, 2021
Version of record online: August 31, 2021

 